Check for updates

Recent advances and perspectives of CeO$_2$-based catalysts: Electronic properties and applications for energy storage and conversion

Xianwei Wang, Jingyi Wang, Yafei Sun, Kanghui Li, Tongxin Shang* and Ying Wan

The Education Ministry Key Laboratory of Resource Chemistry, Joint International Research Laboratory of Resource Chemistry of Ministry of Education, Shanghai Key Laboratory of Rare Earth Functional Materials, Shanghai Frontiers Science Center of Biomimetic Catalysis, Shanghai Non-Carbon Energy Conversion and Utilization Institute, Shanghai Normal University, Shanghai, China

Cerium dioxide (CeO$_2$, ceria) has long been regarded as one of the key materials in modern catalysis, both as a support and as a catalyst itself. Apart from its well-established use (three-way catalysts and diesel engines), CeO$_2$ has been widely used as a cocatalyst/catalyst in energy conversion and storage applications. The importance stems from the oxygen storage capacity of ceria, which allows it to release oxygen under reducing conditions and to store oxygen by filling oxygen vacancies under oxidizing conditions. However, the nature of the Ce active site remains not well understood because the degree of participation of f electrons in catalytic reactions is not clear in the case of the heavy dependence of catalysis theory on localized d orbitals at the Fermi energy E_F. This review focuses on the catalytic applications in energy conversion and storage of CeO$_2$-based nanostructures and discusses the mechanisms for several typical catalytic reactions from the perspectives of electronic properties of CeO$_2$-based nanostructures. Defect engineering is also summarized to better understand the relationship between catalytic performance and electronic properties. Finally, the challenges and prospects of designing high efficiency CeO$_2$-based catalysts in energy storage and conversion have been emphasized.

KEYWORDS

cerium dioxide, catalysts, photocatalysis, electrocatalysis, energy storage and conversion, electronic properties

1 Introduction

Nowadays, most of the energy demand (more than 80%) is met by fossil fuels (such as coal, oil, and natural gas). However, the rapidly growing energy consumption gives rise to serious environmental concerns and energy crisis (Xie et al., 2017). Non-conventional energy sources, such as solar, wind, hydropower, etc., are being considered as possible sources of energy to meet the growing demand and

alleviate environmental destruction (Wang J. et al., 2019). It has been clear for decades that renewable energy sources play important role in the modern grid. While the intermittent nature of these renewable energy sources will lead to a significant mismatch between supply and demand. Electrical energy conversion and storage from different renewable energy sources is a high-efficiency and clean strategy that takes full advantage of all kinds of energy. Many new technologies for energy conversion and storage are under development, which is expected to meet the requirement of their practical applications. Especially, the development of the electrochemical and photochemical processes is a prospective goal to sustainably and cleanly realize the efficient conversion and stora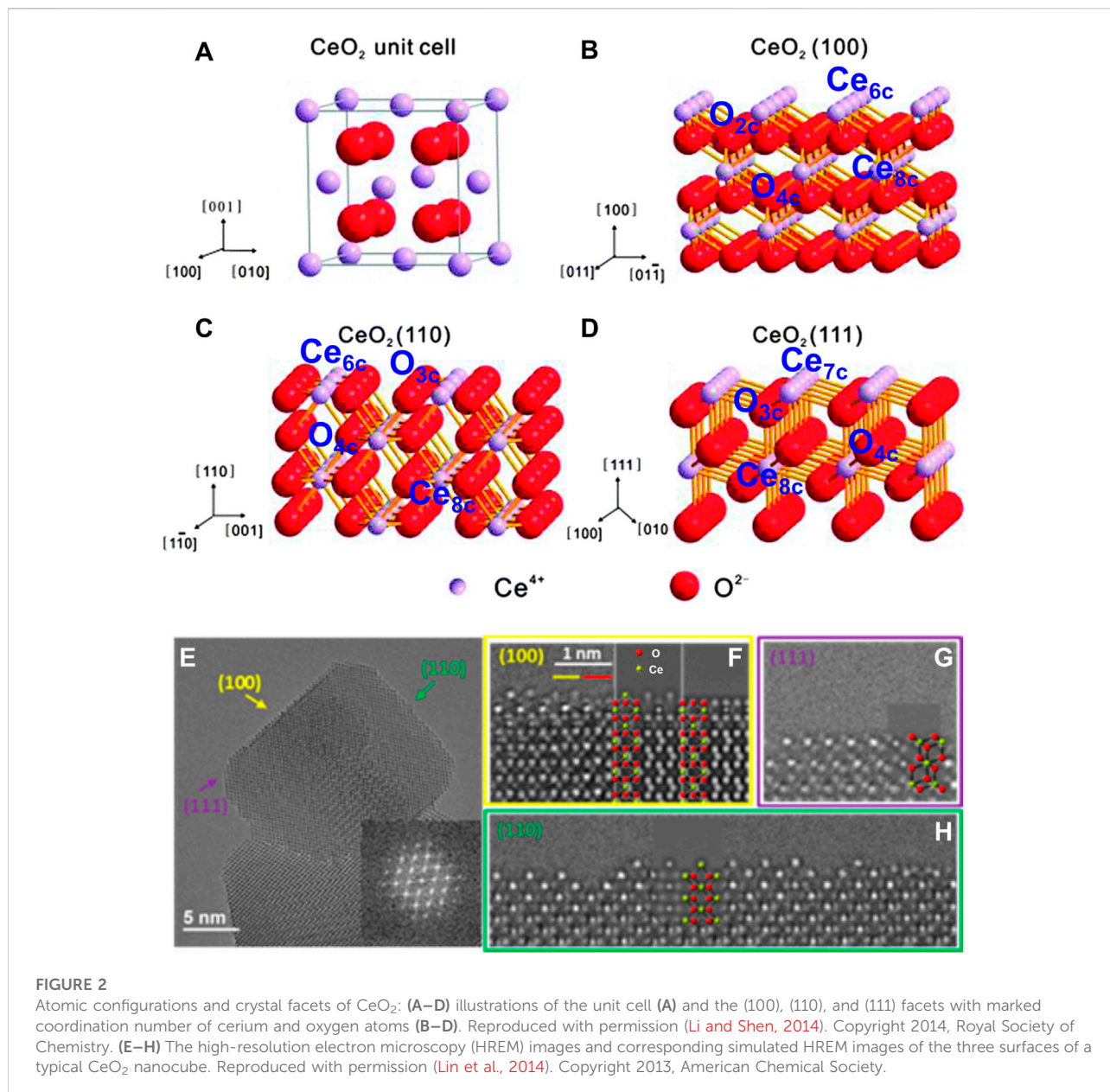ge of many energy molecules, including carbon dioxide and a series of C_{2+} hydrocarbons and oxygenates, hydrogen, sulfur, nitrogen, and so on (Li Q. et al., 2021). To realize this expectation, it is necessary and urgent to develop photo (electro) catalysts with high catalytic activity and improved selectivity towards the high-efficiency energy molecules transformations. Numerous catalysts have been developed for the energy molecules conversion reactions such as carbon dioxide reduction reaction (CO_2RR), hydrogen evolution reaction (HER), oxygen evolution reaction (OER), sulfur reduction reaction (SRR), etc., (Cai et al., 2021). For those important reactions, various carbon-based, metal-based, and metal oxide-based catalysts have been widely investigated. However, their performances, such as activity, stability, cost, and so on, are still need to strengthen. Especially, the conversion efficiency and the selectivity of the developed photocatalysts are still far from satisfactory up to now. Therefore, the development of better catalysts with the necessary selectivity and efficiency for the relevant chemical reactions is urgent.

CeO_2, a widely studied rare Earth oxide, has gained promising applications in photocatalysis and electrocatalytic energy storage and conversion (Montini et al., 2016). Cerium is the most abundant of the rare Earth elements accounting for around 0.0046 wt% of the Earth's crust. CeO_2, as the most common oxide of cerium element, has good stability with a cubic fluorite crystal structure. Specifically, each Ce^{4+} is coordinated with eight adjacent O^{2-} to form an octahedral interstitial, and each O^{2-} is coordinated with four adjacent Ce^{4+} to form a tetrahedral unit in the CeO_2 unit cell (Li and Shen, 2014). CeO_2 possesses unique electronic configurations of $[Xe]4f^15d^16s^2$ resulting in excellent physical and chemical properties, for example, the different colors for the CeO_2 with different stoichiometry due to the charge transfer between Ce^{4+} and O^{2-} (Melchionna and Fornasiero, 2014). The energy of the inner $4f$ level is nearly the same as that of the outer or valence $5d$ and $6s$ levels, thus small amounts of energy can change the relative occupancy of these electronic levels and give rise to a variable electronic structure, which is the intrinsic property for

FIGURE 1
Illustration of electronic properties and catalytic applications of CeO_2.
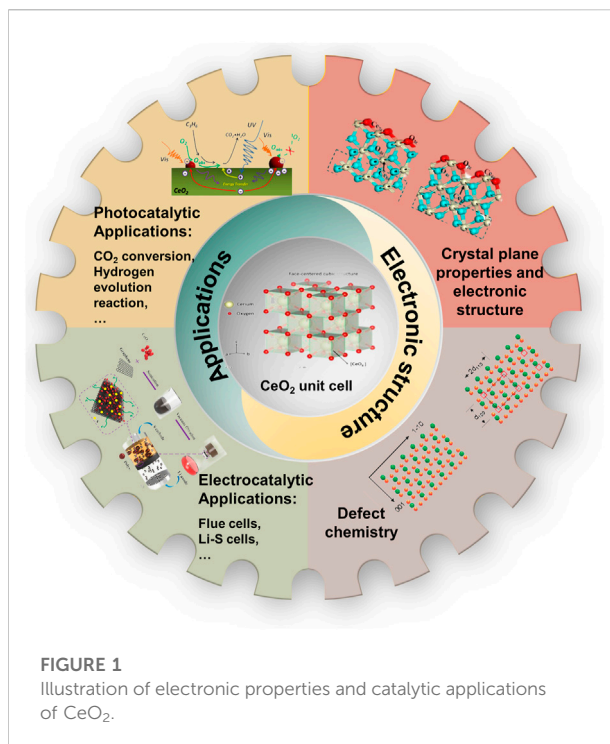
CeO_2 with application potentials in catalysis, energy conversion and storage, and other felids. For non-stoichiometric CeO_{2-x}, four outer electrons of each cerium atom transfer to the two adjacent cerium atoms with the oxygen atom *via* the oxygen p orbital, which is beneficial to the reduction of Ce^{4+} to Ce^{3+} (Shea, 2020). Therefore, Ce^{3+} and Ce^{4+} are steadily exist and facilely switch between these two valence states, and the reversible conversion of the two valence state distributions of cerium ions ensures the formation or elimination of oxygen vacancies. The multivalence property of CeO_2 is the key to achieve the enhanced performances in electrocatalytic and photocatalytic applications, as it benefits to generate strong interactions with reactants or other components in catalysts (Ganduglia-Pirovano et al., 2007; Gao et al., 2017; Li Q. et al., 2021). Besides, the reversible valence characteristics endow the CeO_2 with a better catalytic performance by manipulating the oxygen vacancies concentration to build defect-rich structures (Kong et al., 2020).

CeO_2-based nanostructures have been widely reported. Previously, there are several reviews on the properties, characterizations, and applications of CeO_2 (Ta et al., 2008; Wang H. et al., 2022; Kumaran et al., 2022). However, none of them have summarized the late advances on CeO_2 from a perspective of understanding the relationship between electronic structures and catalytic application. Hence, a timely and focused progress report of CeO_2 electronic properties is expected to further accelerate the development of CeO_2-based emerging materials and promote their diverse applications. In this

FIGURE 2
Atomic configurations and crystal facets of CeO₂: **(A−D)** illustrations of the unit cell **(A)** and the (100), (110), and (111) facets with marked coordination number of cerium and oxygen atoms **(B−D)**. Reproduced with permission (Li and Shen, 2014). Copyright 2014, Royal Society of Chemistry. **(E−H)** The high-resolution electron microscopy (HREM) images and corresponding simulated HREM images of the three surfaces of a typical CeO₂ nanocube. Reproduced with permission (Lin et al., 2014). Copyright 2013, American Chemical Society.

review, we summarize the recent development in the understanding and regulating strategy of electronic properties of CeO₂-based nanostructures. The defects engineering is also summarized to better understand the relationship between catalytic performance and electronic properties. We then overview the catalytic applications of CeO₂-based nanostructures in energy conversion and storage and discuss the mechanisms for several representative catalytic reactions and electrochemical cells in the presence of CeO₂. Finally, the challenges and prospects of designing high efficiency CeO₂-based catalysts in energy storage and conversion have been emphasized (Figure 1).

2 Electronic properties of CeO₂-based nanostructures

2.1 Crystal plane properties and electronic structure

CeO₂ has been widely used as the critical component (active site or support) and electronic promoter in heterogeneous catalysts. Further improving its selectivity and activity for certain reactions hold great promise by the materials engineering methods at the atomic level. It is also important to offer a more detailed understanding of the effects of various

material design methods and the origin of the enhanced reactivity of these modified materials. For CeO_2, the unique electronic configuration and the stable crystalline structure are the essential factors for its catalysis and electrochemical purpose.

CeO_2 is an *n*-type semiconductor with a band gap of about 3.2 eV. CeO_2 nanocrystal presents the fluorite crystal structure with space group *Fm3m* at the temperature range from room temperature to the melting point. As shown in Figure 2A, the fluorite structure consists of a face-centered cubic (f.c.c.) unit cell of cations with anions occupying the octahedral interstitial sites. In a CeO_2 unit cell, each Ce^{4+} is coordinated with eight oxygen ions nearby, and each O^{2-} in the tetrahedral space coordinates with the four nearest Ce^{4+}. Generally, CeO_2 exposes three thermodynamically stable surfaces and the stability follows the order (100) < (110) < (111) according to the surface energy obtained from the density functional theory (DFT) calculations (Figures 2B–D). As shown in Figures 2E–H, the atomic structures of these exposed facets of CeO_2 nanocubes have been observed and determined using aberration-corrected high-resolution electron microscopy by Lin et al. (2014). In comparison to the bulk CeO_2 materials, the cerium and oxygen atoms are unsaturated in all three exposed facets with a lower coordination number and a higher activity. Specifically, the polar (100) surface is terminated by sixfold-coordinated cerium atoms (Ce_{6c}) and twofold-coordinated oxygen atoms (O_{2c}); the (110) surface is terminated by a CeO_2 plane with sixfold cerium (Ce_{6c}) and threefold oxygen atoms (O_{3c}); and the (111) surface is terminated by sevenfold-coordinated cerium atoms (Ce_{7c}) and threefold-coordinated oxygen atoms (O_{3c}) (Spezzati et al., 2019; Zhong and Gong, 2019). The surfaces (111) and (110) have neutral charges, while (100) is made up of a series of charged planes and a dipole moment. The performances in various catalytic reactions of CeO_2-based catalysts are greatly related to their exposed facets, because the chemical state of surface cerium ions and the concentration of oxygen vacancies, which can construct the solid frustrated Lewis pair sites and hence influence the adsorption/activation energy of reactants on the surface, are expected to vary with their hosted facets (Zhang et al., 2017; Zhang Z. et al., 2020; Zhu et al., 2020). Both theoretical and experimental studies have demonstrated that the (100) and (110) surfaces of CeO_2 are more reducible and active than the (111) surface (Trovarelli and Llorca, 2017), which is accordance with the sequence of the vacancy-formation energies (111) > (100) > (110) [2.60 eV for (111) surface, 2.27 eV for (100) surface and 1.99 eV for (110) surface] (Nolan et al., 2005). Amoresi et al. (2019) have synthesized CeO_2 nanocrystals with different exposed crystalline planes by the morphology controlling and found that the hexagon-shaped CeO_2 with dominant (111), (110), and (311) crystal planes has the best photocatalytic efficiency and highest degradation rate of organic pollutants due to its largest band gap energy and the highest (110) and lowest (311) electron density. Shen and co-authors have also investigated the relationships between the

morphologies of CeO_2 nanowires, nanorods, and nanoparticles and their redox and catalytic performances (Tana et al., 2009). The most reactive planes, known as the active (100) and (110) planes, are found in CeO_2 nanorods and nanowires, while the least reactive planes, known as the (111) planes, are located in CeO_2 nanoparticles (Figures 3A–C). As expected, the CeO_2 nanoparticles presented the lowest CO conversion at the low temperature range (Figure 3D). The CeO_2 nanowires dominated by the reactive (110) and (100) planes benefited to expose a large proportion of active planes on the surface, which resulted in a much higher activity for CO oxidation. Besides, Zhang Z. et al. (2020) have demonstrated that the CeO_2 nanorods (r-CeO_2) with the exposed (110) and (100) crystal planes exhibited significantly higher catalytic efficiency and an unheard-before high crotyl alcohol selectivity for selective hydrogenation of crotonaldehyde (Figure 3E). They concluded that surface oxygen vacancies are the active sites for catalyzing crotonaldehyde hydrogenation reaction, which played a key role in controlling the structures of adsorbed C_4H_6O by the formed H^- from heterolytic H_2 dissociation and thus determining the crotyl alcohol selectivity.

Besides the crystal plane properties, many studies of CeO_2 were devoted to clarifying the role of Ce 4*f* electrons under a perspective of electronic structure. It has been demonstrated that surface relaxation and *f* electron localization were believed to be responsible for the observed oxygen vacancy structures and formations. Therefore, understanding Ce 4*f* electrons is important for clearing the distribution of catalytic sites and the catalytic performance of CeO_2 (Li et al., 2009). The ground state electronic structure of CeO_2 has been dealt with two approaches due to the controversy about the occupancy of the Ce 4*f* states. Koelling et al. (1983) have pointed out that some covalent bonding is present in CeO_2 and thus ceria is not completely ionic in early self-consistent field (SCF) band calculations of the bulk CeO_2. Then Fujimori inferred the presence of partial occupancy of the Ce 4*f* states in CeO_2 and concluded that the ground state of ceria might be a mixture of two cerium configurations ($4f^0$ and $4f^1$). Therein, Ce $4f^0$ has a filled O 2*p* valence band and Ce $4f^1$ shows a partially filled O 2*p*-valence-band (Fujimori, 1984). Skorodumova et al. (2001) have reported the DFT calculations of bulk CeO_2 and Ce_2O_3 in the framework of the full-potential linear muffin-tin orbital (FP-LMTO) method and obtained the best agreement with the experiment for CeO_2 by treating the cerium 4*f*-functions as part of the valence region. However, Wuilloud et al. (1984) and Marabelli and Wachter (1987) believed that the cerium 4*f* states in CeO_2 are fully unoccupied and localized. In this case, Ce was treated as tetravalent Ce^{4+} with an unoccupied 4*f*-band ($4f^0$) and a completely filled O 2*p*-band. Under the assumption that the Ce 4*f* orbitals is unoccupied, Hill and Catlow (1993) and Gennard et al. (1999) have neglected completely the Ce 4*f* basis functions and discovered that the bulk properties of CeO_2 were able to be well described even without the Ce 4*f*
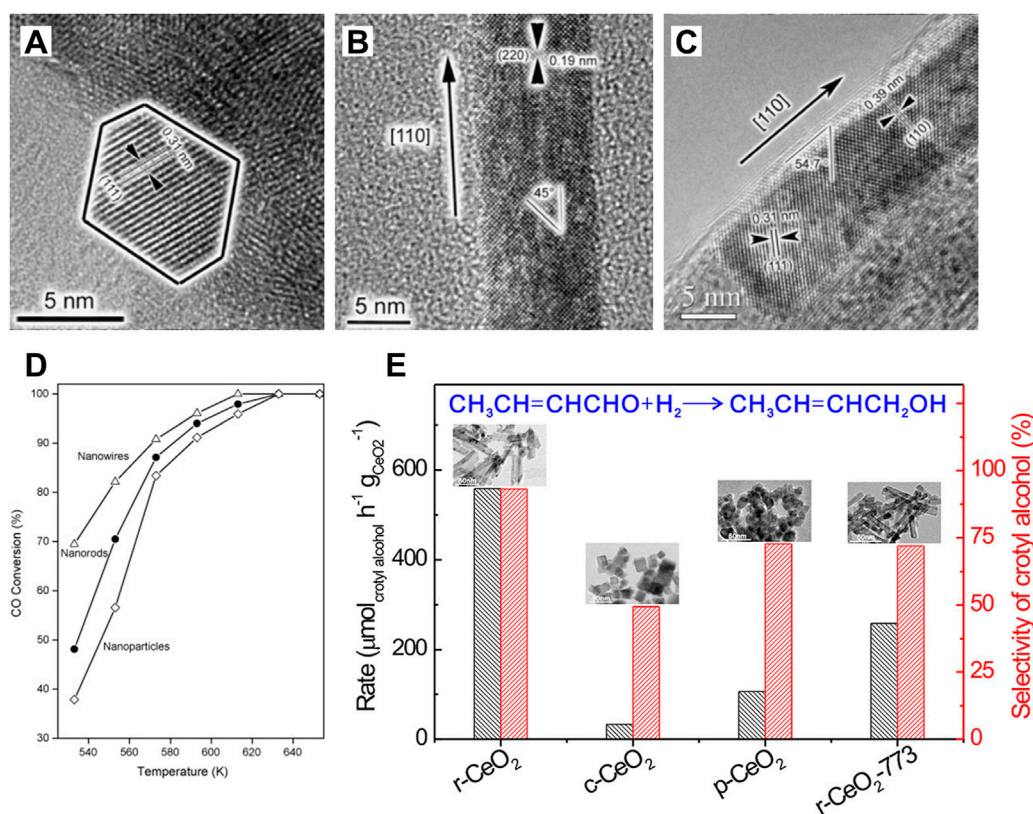
FIGURE 3
Crystal-plane-controlled catalytic performances: **(A−C)** Transmission electronic microscopy images of CeO$_2$ nanoparticles **(A)**, nanorods **(B)** and nanowires **(C)**; **(D)** CO conversions over the CeO$_2$ nanostructures with different morphologies. Reproduced with permission (Tana et al., 2009). Copyright 2009, Elsevier. **(E)** Formation rate and catalytic selectivity of crotyl alcohol for the gas-phase selective hydrogenation of crotonaldehyde catalyzed by various CeO$_2$ at 323 K. Reproduced with permission (Zhang Z. et al., 2020). Copyright 2020, American Chemical Society.

electrons by using a minimal basis set on Ce and O and a more extended basis set, respectively.

2.2 Defect chemistry of ceria

Typically, CeO$_2$ was used as an oxygen buffer in the three-way catalyst, as the quick and reversible redox between Ce^{4+} and Ce^{3+} ensures fast transfer of gaseous oxygen molecules on the solid CeO$_2$ surface. In most studies, the excellent catalytic activity has been directly ascribed to its ability to store and release oxygen, i.e., the oxygen storage capacity (OSC). While the OSC of CeO$_2$ is associated with the efficient supply of lattice oxygen at reaction sites determined by oxygen vacancy formation. Therefore, understanding the vacancy engineering as well as the unique defect thermodynamics of CeO$_2$ at the atomic level is essential to guide the design of CeO$_2$-based catalysts. Defects in the crystal structure are the destruction of the symmetry in the perfectly periodic lattice, which are caused by the displacement of atoms from lattice positions. According to

the dimensionality of the defects, the CeO$_2$ defect can be categorized into point defects (such as oxygen defects and cerium defects) (Esch et al., 2005), line defects (including dislocation defects) (Cao et al., 2022) and plane defects (containing grain boundary defects) (Hojo et al., 2010).

The point defect refers to the vacancies including oxygen and cerium. Among them, oxygen defects have been widely studied due to their simple structure and extensive applications in catalysis. The oxygen defects of CeO$_2$ can be simply divided into intrinsic defects and doped defects according to their origin. Generally, intrinsic defects occur with thermal disorderliness in a crystal following the reductive conversion of Ce^{4+} to Ce^{3+} or the migration of lattice oxygen (Wu et al., 2010; Zacherle et al., 2013; Yang et al., 2021). Doped defects are caused by replacement for normal atoms/ particles or occupation of the interstitial site in normal nodes when introducing heteroatoms/particles. The defect form (oxygen or cerium defects) and concentration can be tuned by changing the valence states of doped ions. A variety of defects can be formed on CeO$_2$ crystal surface with the valence
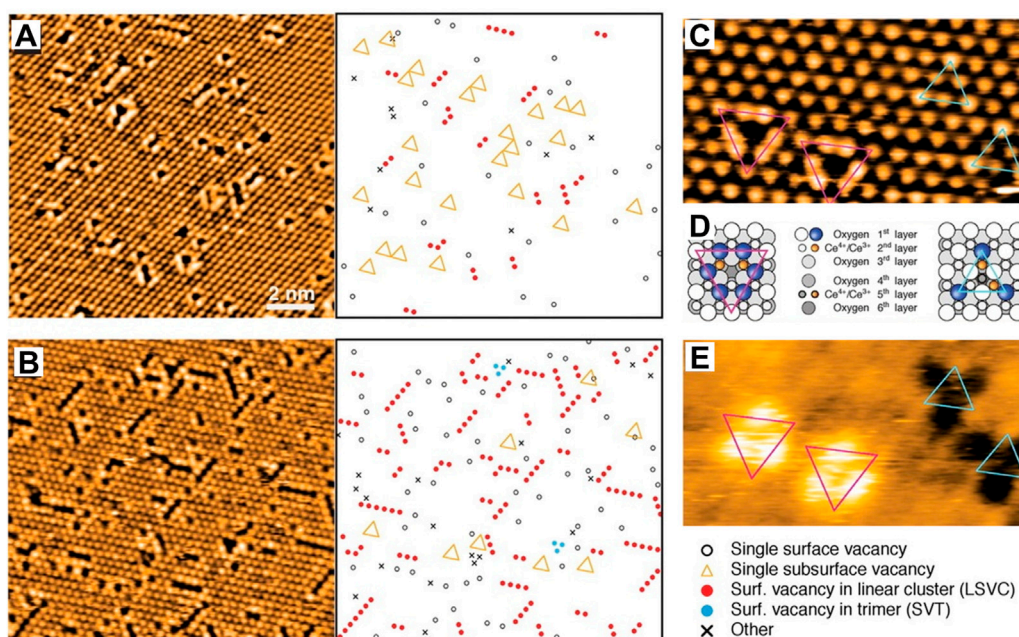
FIGURE 4
Defect formation on the CeO$_2$ (111) surface: **(A,B)** STM images of the CeO$_2$ (111) surface under different reduction degree and corresponding representations of the observed defects. **(C–E)** Filled-state **(C)** and empty-state **(E)** STM images of single vacancies, and related structural models **(D)** (magenta triangles mean the surface vacancy and cyan triangles represent the subsurface vacancy). Reproduced with permission (Esch et al., 2005). Copyright 2005, Science.

state changing of Ce ion, including point defects, as well as line-type and triangular-type defect clusters, resulting from multiple point defects (Fukui et al., 2002). Esch et al. (2005) have systematically studied the local structure of the surface and subsurface oxygen vacancies on the CeO$_2$ (111) facet by using high-resolution scanning tunneling microscopy (STM) and DFT calculations. They found that single vacancies prevail on the slightly reduced surface and linear surface oxygen vacancy clusters appear and grow upon further reduction (Figures 4A,B). On the slightly reduced surface, single vacancies are distinguished to be surface oxygen vacancies and subsurface oxygen vacancies. Upon further reduction, the linear surface oxygen vacancy clusters appear in three different orientations, reflecting the threefold symmetry of the substrate (Figures 4C–E). Specifically, they suggested that electrons localized on cerium ions by releasing oxygen and then clusters of more than two vacancies exclusively expose these reduced cerium ions, primarily by including subsurface vacancies, which therefore play a crucial role in the process of vacancy cluster formation.

As introduced above, the periodically linear permutation of the point defects can be regarded as a line defect, which derives from the periodically crystal destruction in a line area (Hojo et al., 2011). A plane defect is produced by a region deviating from periodicity in a crystal, for example, faulting

and grain boundary. Among, the grain boundary-derived plane defect is the most widespread. Specific grain boundary structures and non-stoichiometry are produced at grain boundaries in oxides because of the structural discontinuity and higher atom energy. These characteristics have significant impacts on the mechanical and electrical properties such as electronic conductivities and oxygen ionization. In order to understand the macroscopic electrical and chemical properties of CeO$_2$, Hojo et al. have investigated the atomic and electronic structures of a (210)Σ5 CeO$_2$ grain boundary by using scanning transmission electron microscopy (STEM) and theoretical calculations (Hojo et al., 2010). They observed that the grain boundary consists of repeating structural units, which were marked by quadrilaterals in Figures 5A–F. The structural units repeat over stretches of an interface length of 10–20 nm accompanied with steps in between these stretches. Although the atomic number for oxygen is too small to clearly observe, oxygen columns were directly identified in the annular bright-field (ABF) image (Figures 5D,F). The non-stoichiometric and stoichiometric grain boundaries were also given as shown in the simulated high-angle annular dark-field (HAADF) images of Figures 5C,E, respectively. Further simulations of the model structures revealed that the stable conditions of non-stoichiometric and stoichiometric grain boundary are the
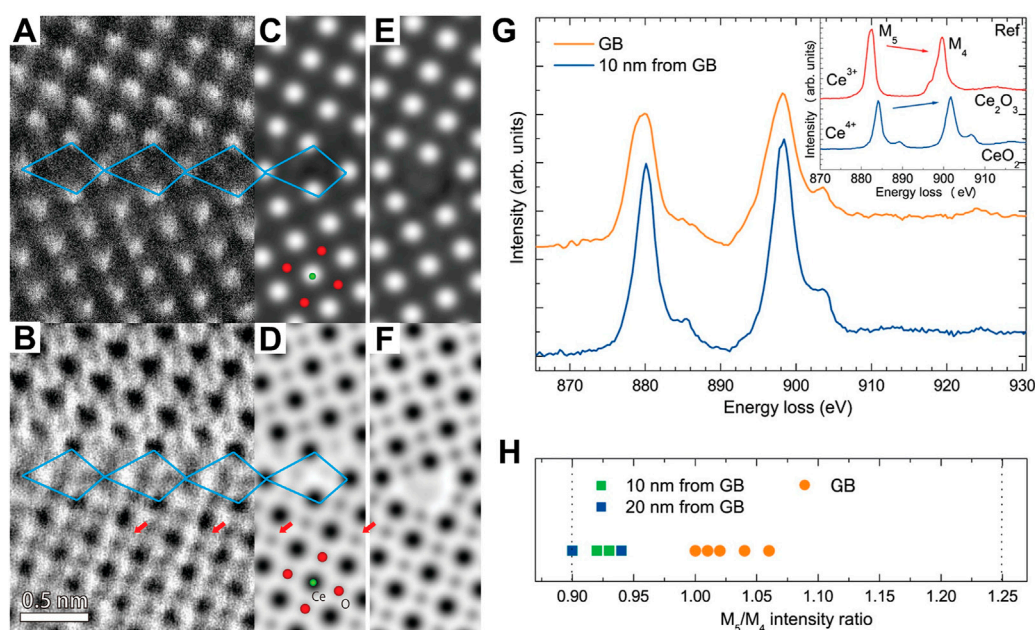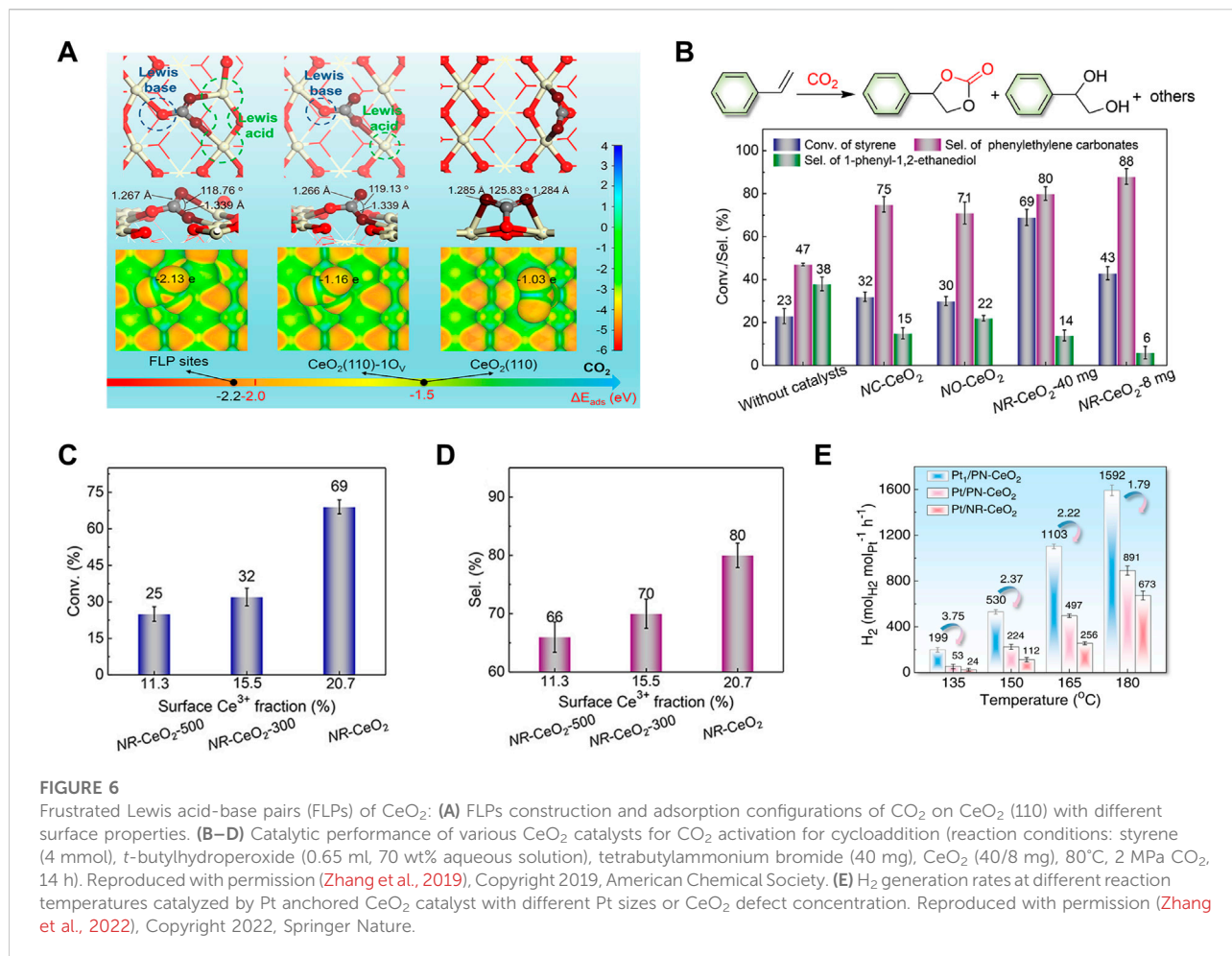
FIGURE 5
Atomic structure of a CeO$_2$ grain boundary: **(A,B)** HAADF **(A)** and ABF **(B)** images of a (210)Σ5 grain boundary in a CeO$_2$ thin film. **(C−F)** Simulated HAADF and ABF images of the non-stoichiometric **(C,D)** and stoichiometric **(E,F)** grain boundary model structure. **(G,H)** Typical Ce M$_{4,5}$-edge EELS spectra taken from the grain boundary and interior region and variation of the M$_5$/M$_4$ intensity ratio at the two different regions. Reproduced with permission (Hojo et al., 2010), Copyright 2010, American Chemical Society.

reducing conditions of $\mu_O < -2.5$ eV and a higher μ_O (i.e., oxidizing conditions), respectively. Accordingly, they inferred that the reducing atmosphere benefits to the preferential formation of the non-stoichiometric grain boundary. By the electron energy-loss spectroscopy (EELS) measurements, they confirmed the presence of oxygen vacancies at the grain boundary and the reduction tendency of the cerium ions at the grain boundary region due to the nearby oxygen vacancies (Figures 5G,H). This work revealed that oxygen non-stoichiometry is significant for the stable grain boundary structure of ceria by sufficient experimental evidence, which paves the way for a comprehensive understanding of grain boundaries through atomic scale determination of atom and defect locations.

Besides, the defect engineering is generally used to construct a frustrated-Lewis-pair (FLP) catalyst. As discussed above, CeO$_2$ (110) exhibits the best reducible and active with the lowest vacancy-formation energy. Similarly, CeO$_2$ (110) presents the highest possibility for FLPs construction (Huang, 2016; Zhang et al., 2017). Many studies have proposed that FLPs constructed on defective ceria possess high activities for many small-molecule activation (such as, H$_2$, NO, CO$_2$) (Mo et al., 2015; Stephan and Erker, 2015; Huang et al., 2018; Li J. et al., 2021; Li et al., 2022; Zhang et al., 2022; Zou et al., 2022). Qu's group have explored the adsorption and activation of CO$_2$ on CeO$_2$ (110) surface by DFT calculations and found that CO$_2$

can be easily activated on defective CeO$_2$ and further activated on FLPs because of the more negatively charged oxygen of CO$_2$, when compared to CO$_2$ on an ideal CeO$_2$ (110) surface (Figure 6A) (Zhang et al., 2019). This group have also prepared a porous nanorods of ceria (PN-CeO$_2$) with mainly exposed (110) and (100) facets and constructed the solid FLPs by controlling surface defects of PN-CeO$_2$ for efficient hydrogenation (Zhang et al., 2017). They concluded that the high concentration of surface defects is important for constructing the FLP sites and improving their capability for H$_2$ activation. As shown in Figure 6A, FLPs are combinations of Lewis acids (the reduced surface cerium atoms) and Lewis bases (the "fixed" surface lattice oxygen) that are sterically prevented from interaction to form Lewis acid-base adjuncts (Zhang et al., 2017; Ma et al., 2018). The surface properties, including electronic structures, defect concentration and spatial distance between Lewis acid and base sites (Ce···O), are critical for construction of a new surface Lewis acidic center (Huang et al., 2018; Ma et al., 2018). Meanwhile, the acidity and basicity of Lewis sites and the spatial distance between Lewis acid and base sites are correlation with the catalytic activity (Stephan and Erker, 2015). There were many works to build the relationship between FLPs and catalytic activities. Zhang et al. compared different CeO$_2$ crystals, including CeO$_2$ nanorods (NR-CeO$_2$) with FLPs, and CeO$_2$ cubes (NC-CeO$_2$) and

FIGURE 6
Frustrated Lewis acid-base pairs (FLPs) of CeO2: **(A)** FLPs construction and adsorption configurations of CO_2 on CeO_2 (110) with different surface properties. **(B–D)** Catalytic performance of various CeO_2 catalysts for CO_2 activation for cycloaddition (reaction conditions: styrene (4 mmol), t-butylhydroperoxide (0.65 ml, 70 wt% aqueous solution), tetrabutylammonium bromide (40 mg), CeO_2 (40/8 mg), 80°C, 2 MPa CO_2, 14 h). Reproduced with permission (Zhang et al., 2019), Copyright 2019, American Chemical Society. **(E)** H_2 generation rates at different reaction temperatures catalyzed by Pt anchored CeO_2 catalyst with different Pt sizes or CeO_2 defect concentration. Reproduced with permission (Zhang et al., 2022), Copyright 2022, Springer Nature.

octahedra (NO-CeO2) without FLPs, to investigate their catalytic performance for cyclic carbonate production from a tandem transformation of olefins and CO_2. These CeO_2 catalysts have the similar surface Ce^{3+} fractions of ~20.8% and surface oxygen vacancy percentages of ~24%. As expected, NR-CeO2 with FLPs delivered the highest styrene conversion and selectivity for cyclic carbonates (Figure 6B). To eliminate the influence of morphology on the formation of FLPs, NR-CeO2 with less surface defect percentages were prepared by calcination at 300°C and 500°C in air. The best activity and highest selectivity were also achieved by the defect-enriched NR-CeO2 sample (Figures 6C,D). Furthermore, they synthesized a porous nanorods of CeO_2 (PN-CeO2) with a high surface Ce^{3+} fraction and obtained an improved selectivity of 94% for cyclic carbonates. Subsequently, Zhang et al. have designed a single-atom Pt anchored PN-CeO2 catalyst (Pt_1/PN-CeO2) with dual-active sites of Pt single-atoms and FLPs on PN-CeO2 to ensure the effective activation of both CH_3OH and H_2O for high efficient H_2 generation at low temperatures (Figure 6E) (Zhang et al., 2022).

3 Applications in energy storage and conversion

3.1 Photocatalytic applications

Photocatalysis is a green chemical pathway with important application prospects in the fields of energy conversion and environmental protection, which has the advantages of simple operation, low energy consumption, no secondary pollution, and high efficiency. Besides, photocatalysis is an important solar fuel production technology due to its potential for producing valuable compounds while mitigating carbon dioxide emissions. In this respect, semiconductor photocatalysis has been widely used in CO_2 reduction (Tran et al., 2022), hydrogen evolution (Dung Van et al., 2021), N_2 reduction to synthesize ammonia (Han et al., 2021), pollutant degradation (Dai Y. et al., 2018), photolysis of water (Wei et al., 2019), etc. In photocatalysis, semiconductors with a smaller half-band gap are more favorable for the photocatalytic reaction and widely used as photocatalysts, whose electrons (e^-) are more easily activated and transferred from the valence band to the conduction band. In the various

photocatalyst semiconductors, TiO_2, CdS, ZnO, MoP, g-C_3N_4, etc., have been extensively investigated (Zhao et al., 2020). As is well-known, the experimental band gap of O $2p \rightarrow$ Ce $4f$ transition is only about 3.2 eV (Corma et al., 2004). On account of its high capacity of store and release oxygen and great chemical stability, CeO_2 is becoming a great promising candidate (Yang et al., 2019). For example, Ji et al. (2008) synthesized ordered mesoporous CeO_2 nano-crystalline and obtained a high photocatalytic activity for the decomposition of the azo dye acid orange under visible light illumination, which greatly outperformed TiO_2 P25. As demonstrated by Arul et al. (2015), the Fe-doped CeO2 hierarchically porous nanostructured showed a great photocatalytic activity for methylene blue degradation under UV–visible light illumination. In this section, the applications in photocatalytic CO_2 conversion and hydrogen evolution reaction of CeO_2-based photocatalysts are overviewed.
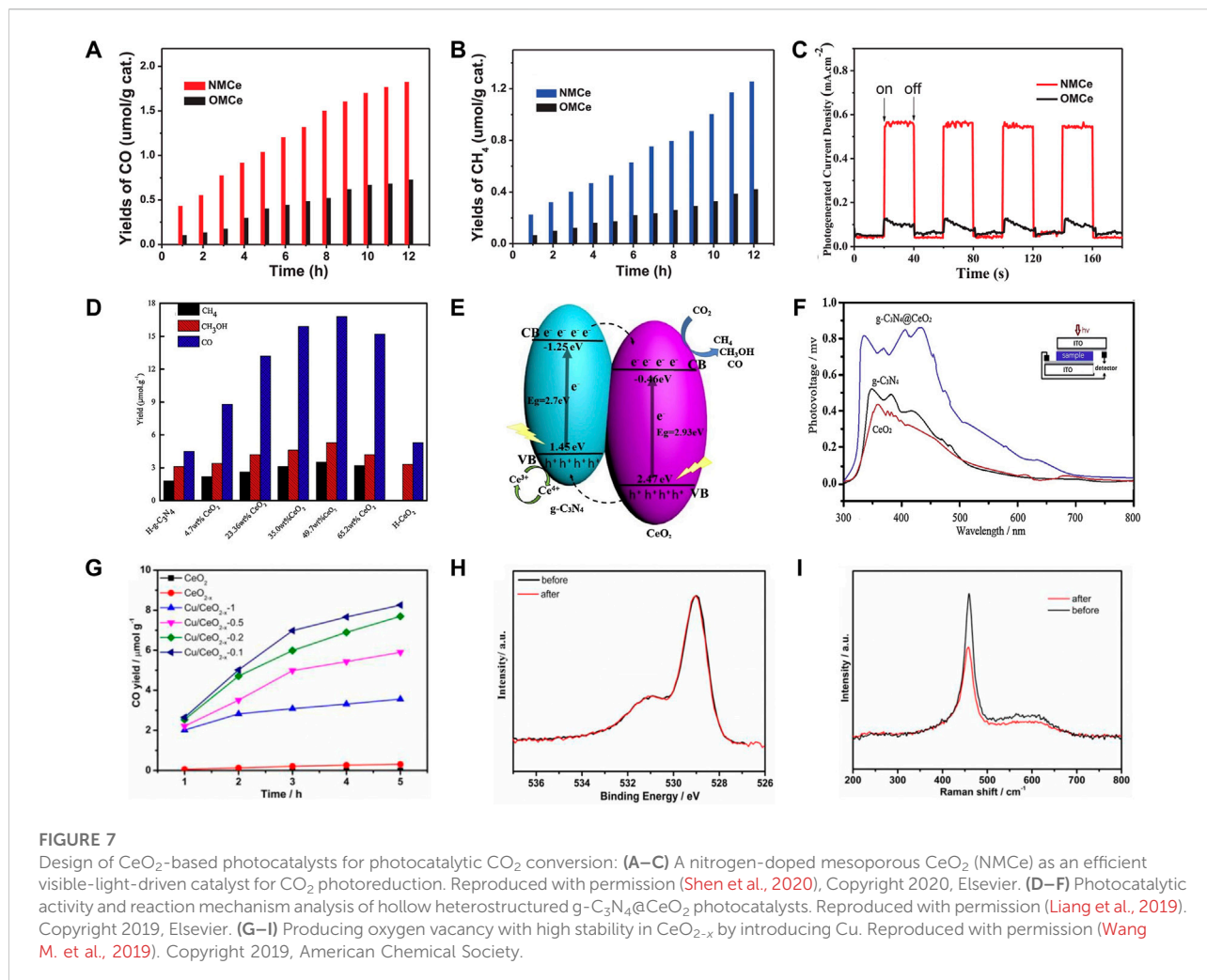
3.1.1 CO$_2$ conversion

In photocatalytic CO_2 conversion, the regulation of structure and the binding site location plays an important role in improving conversion efficiency. Oxides of rare Earth metals not only exhibit an excellent capability during the CO_2 adsorption process, but also present a high charge separation efficiency *via* the addition of surface oxygen vacancies (Muhammad et al., 2020). Hence, rare Earth metals have been considered as the highly viable options for photocatalytic CO_2 conversion. Ceria was widely studied due to its high chemical stability and outstanding oxygen storage-and-release capability. Besides above mentioned advantages, Fiorenza and co-workers have further emphasized the photocatalytic capability of ceria. They pointed out that the combination of light and temperature can greatly enhance the performance of ceria photocatalysis (Fiorenza et al., 2022). Despite the intrinsic ability of pristine CeO_2, a higher CO_2 conversion performance is desired by the optimization of the conduction band (CB) position and quick electron-hole recombination. To achieve high activity and product selectivity in photocatalytic CO_2 conversion, numerous catalysts modified techniques, such as metal or non-metal doping (Wang M. et al., 2022), building heterojunction (Hamidah Abdullah et al., 2017), and oxygen vacancy engineering (Hezam et al., 2020), have been reported, which benefit to promote CO_2 molecule activation and adsorption. We mainly summarized the improved CeO_2-based photocatalysts through element doping, heterojunction building and vacancy engineering in this section.

Elements doping has impacts on the electronic structures of the semiconductor photocatalyst, particularly the bandgap. Transition metal are the common dopant elements for optical and photoelectrochemical semiconductor modification, among which the most widely used include Fe, Ni, Cr, Ag, and so on (Wang Y. et al., 2019; Prajapati et al., 2022). Through the dispersion of Ag particles on CeO_2 surfaces, Cai and

co-authors have investigated the impact of surface plasmon effect on photocatalytic CO_2 conversion efficiency. It is noteworthy that the Ag-CeO_2 photocatalyst, which was created *via* a straightforward solvent-based method, can simultaneously produce CH_4 and CH_3OH after 6 h of visible light irradiation, giving 100 and 35 mol·g^{-1} h^{-1} of CH_4 and CH_3OH, respectively (Cai et al., 2018). Furthermore, in numerous studies, non-metal doping has been mentioned as a viable method to improve photocatalytic activity. Non-metal-loaded elements that could widen the absorption zone to absorb visible light include nitrogen (N) (Shen et al., 2020), sulfur (S) (Wang et al., 2021), and phosphate (P) (Li W. et al., 2021). Excellent CO_2 reduction was demonstrated by nitrogen-doped CeO_2, with CO and CH_4 yields of 1.83 and 1.25 μmol·g^{-1}, respectively, being 2.5 times higher than those of nanocasted ordered mesoporous CeO_2 (OMCe) (Figures 7A–C) (Shen et al., 2020).

The photocatalytic efficiency of pure CeO_2 as a photocatalyst is insufficient. Heterojunction of CeO_2 and other nanomaterials is able to overcome the limitations of single component and lead to the synergistic effect, which has been considered as one of the most promising structures to improve its photocatalytic activity. Heterojunction possesses a great benefit in separating photoinduced (e)—(h+) pairs and takes full advantage of the individual functional properties of each component (Zhang W. et al., 2020). Dai and co-workers prepared the CeO_2/Bi_2MoO_6 heterostructured microspheres with different CeO_2 contents *via* a facile solvothermal route. The heterojunction of CeO_2/Bi_2MoO_6 nanocomposite showed a high specific surface area and a significantly enhanced response to visible light, which is conductive to improve the charge carrier separation and transfer efficiency. As a result, 5% CeO_2-Bi_2MoO_6 with the best activity in photocatalytic CO_2 reduction toward the generation of CH_3OH and C_2H_5OH realized the yields of 32.5 and 25.9 μmol·g$_{cat}$$^{-1}$ for CH_3OH and C_2H_5OH, respectively (Dai W. et al., 2018). Layered graphitic carbon compound (g-C_3N_4) exhibits wonderful photocatalytic activity due to its high reducibility and visual lightweight absorption, but the low specific area and speedy charge recombination in pristine g-C_3N_4 have prevented its practical use (Bian et al., 2018). Liang et al. (2019) designed a hollow g-C_3N_4@CeO_2 heterostructure photocatalyst with abundant oxygen vacancies to enhance light utilization and catalytic activities. Because of the unique structure, the synergetic effect and oxygen vacancies, g-C_3N_4@ CeO_2 makes multiple reflections of light in the cavity and contributes greatly to the enhanced CO_2 adsorption capability, thus achieving a much earlier CH_4 generating and a higher CH_4 concentration in comparison to that of the pristine g-C_3N_4 and CeO_2. The g-C_3N_4@CeO_2 with a CeO_2 loading of 49.7 wt% showed the best CO_2 photoreduction performance with the yields of CH_3OH (5.2 μmol·g^{-1}), CO (16.8 μmol·g^{-1}) and CH_4 (3.5 μmol·g^{-1}) (Figure 7D). Further mechanism analysis deduced that the photogenerated electrons in the CB of the g-C_3N_4 are able to migrate to the CB of the CeO_2 while the holes generated in

FIGURE 7
Design of CeO$_2$-based photocatalysts for photocatalytic CO$_2$ conversion: **(A−C)** A nitrogen-doped mesoporous CeO$_2$ (NMCe) as an efficient visible-light-driven catalyst for CO$_2$ photoreduction. Reproduced with permission (Shen et al., 2020), Copyright 2020, Elsevier. **(D−F)** Photocatalytic activity and reaction mechanism analysis of hollow heterostructured g-C$_3$N$_4$@CeO$_2$ photocatalysts. Reproduced with permission (Liang et al., 2019). Copyright 2019, Elsevier. **(G−I)** Producing oxygen vacancy with high stability in CeO$_{2-x}$ by introducing Cu. Reproduced with permission (Wang M. et al., 2019). Copyright 2019, American Chemical Society.

the CeO$_2$ will transfer to the valence band (VB) of the g-C$_3$N$_4$ for the g-C$_3$N$_4$@CeO$_2$ composites (Figure 7E). Such interfacial electron transfer contributes greatly to the separation efficiency of electron-hole pairs resulting and thus the accumulated electron-hole pairs on the CeO$_2$ surface promote the generation of CH$_4$, which was demonstrated by the obvious surface photovoltage spectroscopy (SPS) signal in visible light region of g-C$_3$N$_4$@CeO$_2$ (Figure 7F). This work provides a novel approach to produce g-C$_3$N$_4$-based photocatalysts in the absence of noble metal for the high efficiency CO$_2$ photocatalytic reduction and clear the charge transfer and catalytic mechanism from the perspectives of structural design and atomic-level regulation.

The poor photocatalytic CO$_2$ performances on pure CeO$_2$ are mainly due to its wide band gap and low light absorption (Xie et al., 2017). Therefore, oxygen vacancy introduction in the CeO$_2$ nanocrystal structure also has attracted strong interest, which can enhance visible-light absorption ability. Introducing oxygen vacancies can make CO$_2$ molecules more easily adsorbed and

activated on the photocatalyst surface due to the abilities of providing active sites and increasing the CO$_2$ adsorption energy. Furthermore, the defect energy level generated by oxygen vacancies is supposed to promote the separation and suppress the recombination of electron-hole and change the transfer path of carriers (Wang et al., 2020). Lai et al. (2022) have introduced surface oxygen vacancies by preparing porous iron-doped ceria, which significantly improved the light absorption performance of ceria in the application of photocatalytic CO$_2$ conversion. In spite of introducing oxygen vacancies is able to significantly enhance the CO$_2$ photoreduction performance of CeO$_2$, its activity would decrease because the stability of the generated oxygen vacancies is insufficient with gradually filling or losing during the photoreduction process. In order to achieve and maintain a high CO$_2$ reductive activity of CeO$_2$, Wang and co-workers introduce Cu into CeO$_2$ to generate and stabilize oxygen vacancies (CeO$_{2-x}$) (Wang M. et al., 2019). They found that the Cu-introduced sample show a lower photoluminescence intensity, indicating the extremely enhanced charge transfer
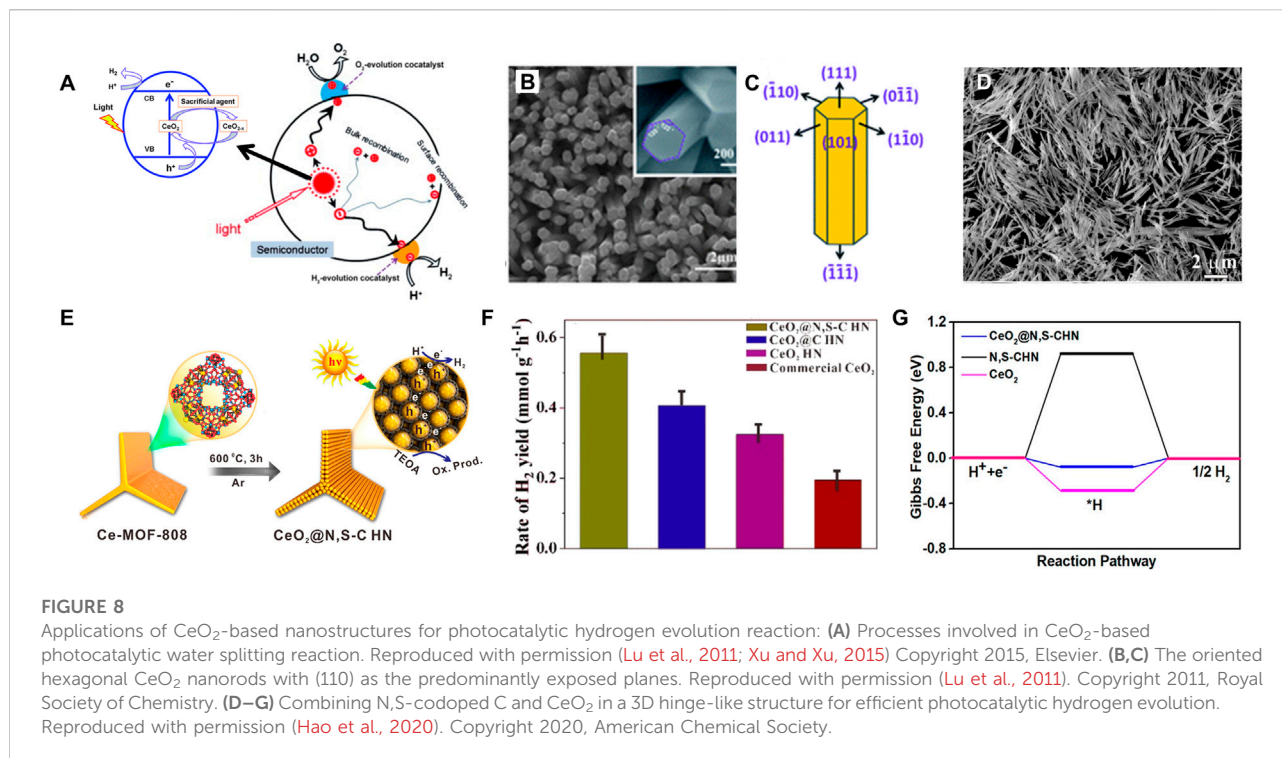
between CeO_2 and Cu species and the effectively inhibited electron-hole recombination, thus leading to a prolonged carriers' lifetime and stabilized oxygen vacancies. By further catalytic mechanism analysis, they proposed the possible reaction mechanism of photocatalytic CO_2 conversion on the Cu/CeO_{2-x} catalysts and confirmed that the introduction of Cu alters the configurations of the adsorbed CO_2 on CeO_{2-x}. Therein, Cu/CeO_{2-x}-0.1 presented the best photocatalytic performance with a CO yield of $8.25\ \mu mol \cdot g^{-1}$ during 5 h of Xe-light irradiation and excellent chemical stability (Figures 7G–I).

3.1.2 Photocatalytic hydrogen evolution reaction

Because of the concerns on the sustainability of fossil fuels, photocatalysis is always research focus to create effective, sustainable, and varied energy storage technologies. H_2 is considered as a promising renewable energy source due to its high energy density of $143\ kJ \cdot g^{-1}$ and the advantages of low emission and no pollution (Xu and Xu, 2015). For a long time, most of the H_2 is produced by hydrocarbon steam reforming or coal gasification, which are high energy-consuming (Zhao et al., 2020). Currently, the photocatalytic hydrogen evolution reaction (HER) has been considered as a prospective approach to produce H_2 by an environment-friendly way and attracted lots of research. However, HER is a multielectron, endothermic uphill reaction that requires a high positive Gibb's free energy (Sultana et al., 2021). Generally, 2.458 eV energy is required to split one water molecule to generate one hydrogen molecule, thus a highly active photocatalyst that possesses capability of decreasing the energy barrier is necessary. Numerous semiconductor photocatalysts with a narrow bandgap and imperative photoredox behavior have been applied in the photolytic HER. Recently, on account of the easy conversion between Ce^{3+} and Ce^{4+} and abundant oxygen vacancies, CeO_2 has been used in the photocatalytic HER. Dong et al. have synthesized the CeO_2 nanorods and found that the pure CeO_2 presented a favorable photocatalytic activity with a high H_2 production rate of $\sim25.10\ \mu mol \cdot g^{-1}$ (after solar light irradiation for 5 h) (Dong et al., 2018). Moreover, a variety of CeO_2-based nanostructures, such as Au/CeO_2 (Primo et al., 2012), ZnO/CeO_2 (Zeng et al., 2014), $CeO_2/g\text{-}C_3N_4$ (Zou et al., 2017), etc., were reported to strengthen the photocatalytic activity of HER. In this section, we overviewed the mechanism of photocatalytic water splitting for H_2 production on CeO_2-based catalysts. Meanwhile, applications of various CeO_2-based nanostructures in photocatalytic HER were summarized from pristine CeO_2 to element-doped CeO_2 and CeO_2-based heterostructure.

As introduced by previous reports, water splitting over ceria mainly includes water hydroxylation and H_2 formation. As shown in Figure 8A, water molecule first adsorbs by the oxygen atom on the top of the cerium atom of CeO_2 (111) and
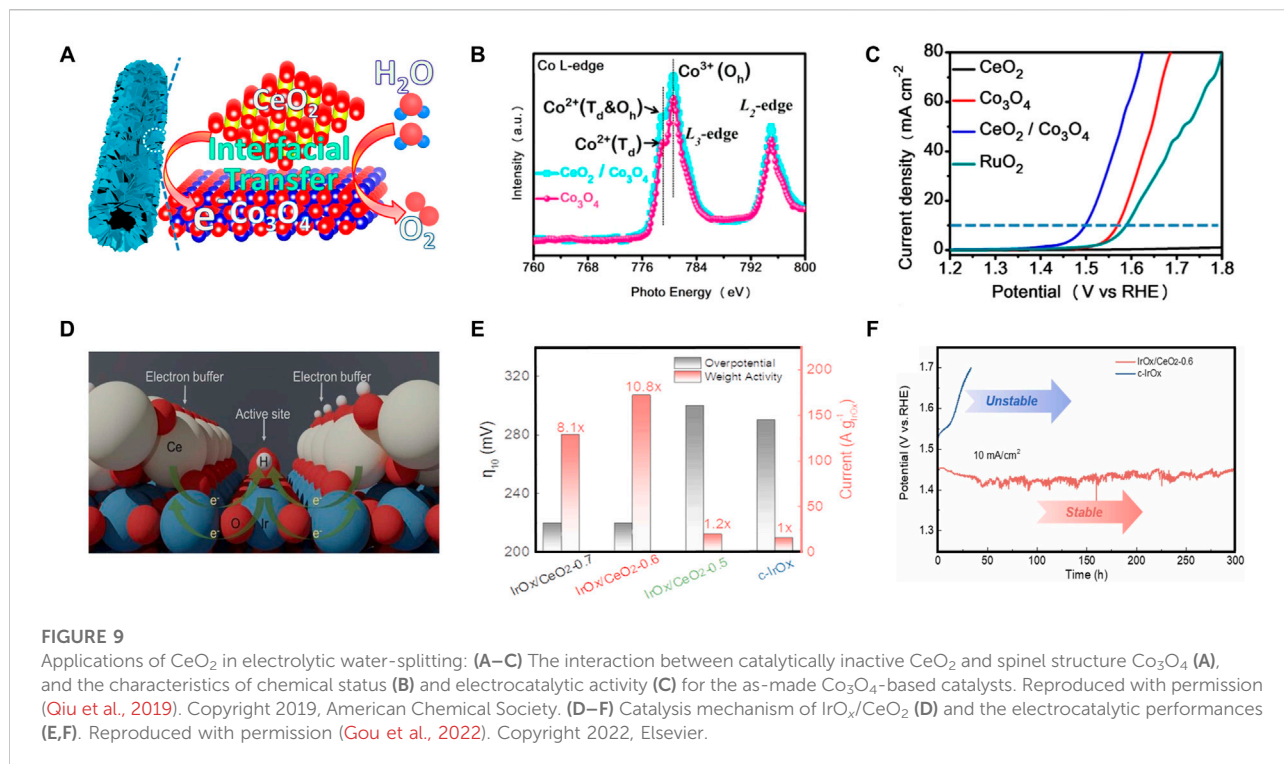
occurs dissociation near the oxygen vacancy of defect enriched CeO_2 (111) accompanied by the bonding between one hydrogen atom of water and the surface oxygen atom of CeO_2. Water dissociation into hydroxyl occurs, followed by hydroxyl decomposition and H_2 liberation through an asymmetric process. Therein, the surface vacancies facilitate the water dissociation step and the process is accompanied by the oxidation of Ce^{3+} to Ce^{4+} (Lu et al., 2011; Chen et al., 2013; Hansen and Wolverton, 2014; Wu et al., 2019). Because different CeO_2 facets show different oxygen and cerium coordination, many studies have developed CeO_2 nanostructures with highly active exposed crystal planes in photocatalytic HER. Tong and co-authors prepared the oriented hexagonal CeO_2 nanorods with (110) as the predominantly exposed planes by a facile electrochemical method (Figures 8B,C) (Lu et al., 2011). Hexagonal CeO_2 nanorods present an excellent redox capability thus a super photocatalytic activity for HER. The H_2 evolution rate on CeO_2 nanorods was about $741\ \mu mol\ g^{-1}\ h^{-1}$ with $Na_2S\text{-}Na_2SO_3$ sacrificial agents, which was much higher than that of the commercial CeO_2 or CdS. However, the photocatalytic efficiency of pure CeO_2 is still not desirable on account of the rapid electron-hole recombination and low proportion of surface active sites. Therefore, non-metallic element doped CeO_2 and CeO_2-based heterojunction structures have been extensively studied. Hao et al. synthesized a N,S-doped C-encapsulated CeO_2 hinge-like nanostructure (CeO_2@N,S-C HN) to improve the separation efficiency of photoinduced electrons-hole pairs and expose more accessible active sites in the photocatalytic reactions (Figures 8D,E) (Hao et al., 2020). The CeO_2@N,S-C HN showed a mass-normalized rate of H_2 production of $555\ \mu mol\ h^{-1} \cdot g^{-1}$, which is remarkably higher than that of CeO_2@C HN ($405\ \mu mol\ h^{-1} \cdot g^{-1}$), CeO_2 HN ($325\ \mu mol\ h^{-1} \cdot g^{-1}$), and commercial CeO_2 ($195\ \mu mol\ h^{-1} \cdot g^{-1}$) (Figure 8F). Moreover, the CeO_2@N,S-C HN had a long-term stability without visible activity degeneration after four cycles. Through the spin-polarized DFT calculations, they found that the CeO_2@N,S-C HN with a lower Gibbs free energy for the formation of the intermediate state (H*) of 0.08 eV exhibited the best HER performance in comparison to pristine CeO_2 (0.30 eV) and N,S-C (0.93 eV) (Figure 8G). They further deduced that the strong interaction between N,S-C HN and CeO_2 (111) was beneficial to the photogenerated carriers transfer and separation, thereby enhancing the catalytic performance for HER. In order to reduce the bandgap energy and enhance plasmonic characteristics toward the visible-light range, introducing nitrogen dopants (such as substitutional and interstitial N sites) to ceria is often used, which can increase oxygen vacancies and Ce^{3+} active defects. Van Dao et al. (2021) synthesized a nitrogen-doped ceria coupled with nitrogen-doped graphene (3.9% $N\text{-}CeO_2$/N-Gr), which exhibited better photocatalytic properties than $N\text{-}CeO_2$ and CeO_2. In this case, a super HER rate of

FIGURE 8
Applications of CeO$_2$-based nanostructures for photocatalytic hydrogen evolution reaction: **(A)** Processes involved in CeO$_2$-based photocatalytic water splitting reaction. Reproduced with permission (Lu et al., 2011; Xu and Xu, 2015) Copyright 2015, Elsevier. **(B,C)** The oriented hexagonal CeO$_2$ nanorods with (110) as the predominantly exposed planes. Reproduced with permission (Lu et al., 2011). Copyright 2011, Royal Society of Chemistry. **(D–G)** Combining N,S-codoped C and CeO$_2$ in a 3D hinge-like structure for efficient photocatalytic hydrogen evolution. Reproduced with permission (Hao et al., 2020). Copyright 2020, American Chemical Society.

3.7 $\mu mol \cdot mg_{cat}^{-1} \cdot h^{-1}$ under visible-light irradiation and remarkable durability were realized by the obtained N-CeO$_2$/N-Gr photocatalyst. The reduced bandgap energy confirmed by the DFT calculations can be ascribed to the synergistically electronic effects between 3.9% N-CeO$_2$ and N-Gr. Besides, the unique structure with a N-Gr shell, N-Gr network and 3.9% N-CeO$_2$ core benefits to play the best role for every component. For the N-CeO$_2$/N-Gr photocatalyst, the N-CeO$_2$ possesses more oxygen vacancies and Ce^{3+} active defects for enhancing plasmonic properties in the visible-light range; and the N-Gr perfectly performs as an electron reservoir to accumulate plasmon-induced electrons traveling from 3.9% N-CeO$_2$ and to suppress the recombination of photoinduced electron-hole pairs. The photocatalytic performance of the heterojunctions is strongly influenced by the interfacial contact between the CeO$_2$ and the other semiconductors (Xu et al., 2014). Therefore, CeO$_2$ is often combined with other photocatalysts/co-catalysts. Shen and co-authors composited CeO$_2$ with W$_{18}$O$_{49}$ to prepare the novel Z-scheme heterojunction photocatalyst W$_{18}$O$_{49}$/CeO$_2$. The W$_{18}$O$_{49}$/CeO$_2$ composite showed a high hydrogen production efficiency of ~0.2061 mmol$\cdot$g$^{-1}\cdot$h^{-1}, which was about 1.93 times higher than that of the pure CeO$_2$. They proved that the Z-scheme heterojunction structure at the contact interface of W$_{18}$O$_{49}$ and CeO$_2$ greatly increased the accumulation of photo-generated electrons and the separation efficiency of the charge carriers, thus enhancing the photocatalytic performance for hydrogen evolution.
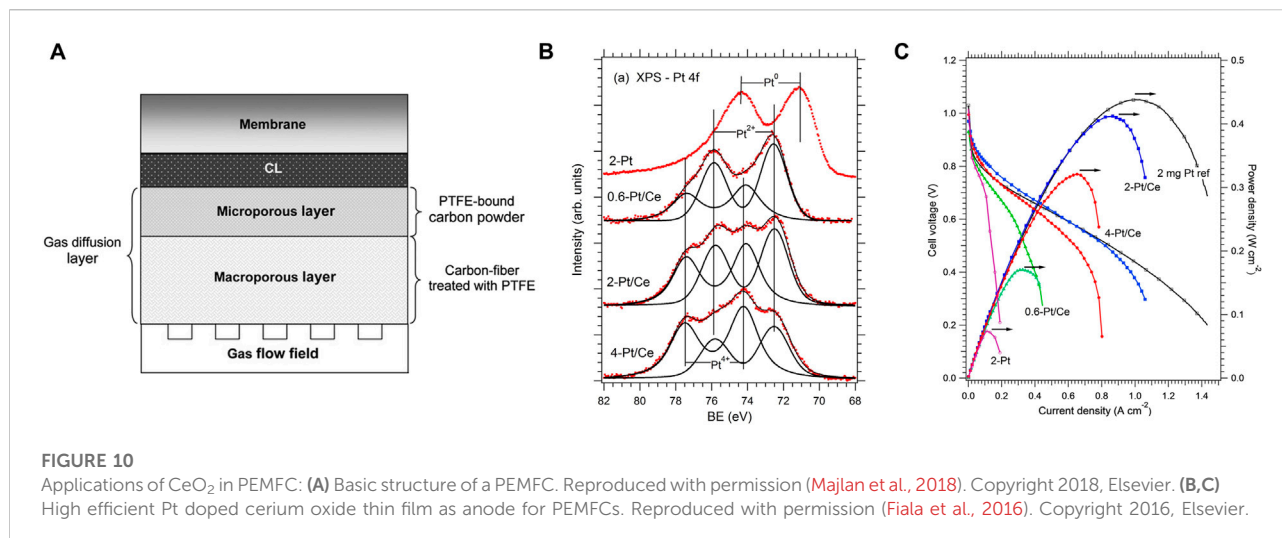
3.2 Electrocatalytic applications

Electrocatalysis as a promising energy conversion technique has attracted extensive attention worldwide, which provides a clean and convenient route to transfer the universal sources into value-added chemicals and storage chemical energy *via* battery systems. In the last decades, remarkable efforts have been devoted to the development of cost-efficient electrocatalysts for related reactions such as hydrogen evolution reaction (HER), hydrogen oxidation reaction (HOR), oxygen evolution reaction (OER), oxygen reduction reaction (ORR), methanol/ethanol oxidation reaction, carbon dioxide reduction reaction, nitrogen reduction reaction and sulfur reduction reaction. Currently, noble metals (like Pt or Ru) and noble metal oxides (like IrO$_2$ or RuO$_2$) are the most outstanding electrocatalysts for these catalytic processes. However, the insufficient reserves and high cost of these materials limit their practical uses (Danilovic et al., 2014). Moreover, the catalytic activity and selectivity for targeted products of these reported electrocatalysts still need to be strengthened. CeO$_2$ with a series of unique properties as summarized above has been exploited as an effective and promising electrocatalyst or catalyst support in many electrocatalysis systems in recent years (Wang J. et al., 2019). In this section, the applications of CeO$_2$-based electrocatalysts in different electrocatalytic reaction of several representative electrochemical systems, including electrolytic water-splitting devices, proton exchange membrane fuel cells, solid oxide fuel cells and lithium-sulfur batteries, are overviewed.

FIGURE 9
Applications of CeO_2 in electrolytic water-splitting: **(A–C)** The interaction between catalytically inactive CeO_2 and spinel structure Co_3O_4 **(A)**, and the characteristics of chemical status **(B)** and electrocatalytic activity **(C)** for the as-made Co_3O_4-based catalysts. Reproduced with permission (Qiu et al., 2019). Copyright 2019, American Chemical Society. **(D–F)** Catalysis mechanism of IrO_x/CeO_2 **(D)** and the electrocatalytic performances **(E,F)**. Reproduced with permission (Gou et al., 2022). Copyright 2022, Elsevier.

3.2.1 Electrolytic water-splitting devices

Splitting water electrochemically and its reversed process form hydrogen and oxygen cycle for energy storage and energy conversion, which involve four critical half-cell reactions, i.e., the HER and oxygen evolution reaction (OER) for energy storage by water electrolysis, and the hydrogen oxidation reaction (HOR) and oxygen reduction reaction (ORR) for energy conversion in fuel cells. Photocatalytic HER is a promising approach to producing H_2 in an environment-friendly way, CeO_2-based photocatalysts for HER have been overviewed in the previous section of photocatalytic applications. In this section, we mainly focus on the OER in the water-splitting process. Because of the slow kinetics of the four-electron process, it is generally known that the OER is the bottleneck in the water-splitting processes. In this regard, it is of a great desire to design active OER catalysts that can accelerate O-H bond breaking and O-O bond formation (Gao et al., 2018; Zhang et al., 2021). On account of its superior ionic conductivity and large oxygen storage capacity, CeO_2 is frequently utilized as a cocatalyst to enhance the charge transfer and energy conversion efficiency of OER catalysts, as well as the OER kinetics (He et al., 2019). The synergistic effect, high surface area, and unique structure of the catalyst all contribute to the enhanced activities (Zhao et al., 2018). Cobalt-based spinel oxides, as one of the promising OER electrocatalysts in alkaline medium, show limited catalytic activity due to the abundant existence of relatively inactive Co^{3+} octahedral coordination (Wang et al., 2016). Qiu and co-workers have built the CeO_2-induced interfacial Co^{2+} octahedral sites and

oxygen vacancies to improve the OER performance of Co_3O_4 (Figure 9A) (Qiu et al., 2019). As shown in Figure 9B, the ratio of Co^{3+}/Co^{2+} in CeO_2/Co_3O_4 was lower than that of the pristine Co_3O_4, accompanied by the increased ratio of Ce^{4+}/Ce^{3+} and oxygen vacancies, which was evidenced by X-ray photoelectron spectroscopy (XPS) and Co L-edge X-ray absorption near-edge structure (XANES). As expected, CeO_2/Co_3O_4 interfacial nanotubes show excellent OER performance with an obviously decreased overvoltage of 265 mV at a current density of 10 mA·cm^{-2}, which is much lower than those of Co_3O_4 (340 mV) and commercially available RuO_2 catalysts (360 mV) (Figure 9C). Meanwhile, CeO_2/Co_3O_4 interface nanotubes with a Ce/Co ration of 2:20 can achieve an ultrahigh mass activity with a current density of 128.6 A·g^{-1} at a given overpotential of 340 mV and enable an OER Faradaic efficiency of ~99%. Li et al. (2022) have reported a very different conclusion on the valence of active Co ions by using CeO_2 nanoparticles anchored Co layered double hydroxide (LDH) as a catalyst. They deemed that the Co^{3+} with strong Lewis acidity helps the binding of OH^- and thus benefiting the formation and transformation of oxygen-containing intermediates by forming CoOOH active species (Li Z. et al., 2021). Besides the electrochemical water-splitting in alkaline electrolyzers, the proton exchange membrane water electrolyzers show more promise for practical applications and have benefits for overall water-splitting. However, OER electrocatalysts in acidic conditions are facing great challenges in their longevity on account of the highly oxidizing and

FIGURE 10
Applications of CeO$_2$ in PEMFC: **(A)** Basic structure of a PEMFC. Reproduced with permission (Majlan et al., 2018). Copyright 2018, Elsevier. **(B,C)** High efficient Pt doped cerium oxide thin film as anode for PEMFCs. Reproduced with permission (Fiala et al., 2016). Copyright 2016, Elsevier.

corrosively acidic operating environments. Gou and co-workers have prepared the amorphous IrO$_x$/CeO$_2$ nanowire electrocatalysts, featured by nanoscale intimacy and amorphous structure, for water oxidation in 0.5 M H$_2$SO$_4$, which are providing abundant binary interfaces and favorable kinetics for acidic OER (Gou et al., 2022). They pointed out that CeO$_2$ as an electron buffer can not only regulate the adsorption of oxygen intermediates and lowers the activation barrier of OER, but also suppress the over-oxidation and dissolution of iridium (Figure 9D). As a result, IrO$_x$/CeO$_2$ significantly enhanced the OER activity and stability. Iridium/CeO$_2$ ratios of 0.6 M (IrO$_x$/CeO$_2$-0.6) delivered the best electrocatalytic OER performances with a high mass activity of 167 A g$_{Ir}^{-1}$ at 1.51 V, a low overpotential of 220 mV at 10 mA·cm^{-2}, and a stable performance for 300 h of continuous operation in acid (Figures 9E,F). This work provides a reasonable strategy for constructing acid-resistant OER electrocatalysts.

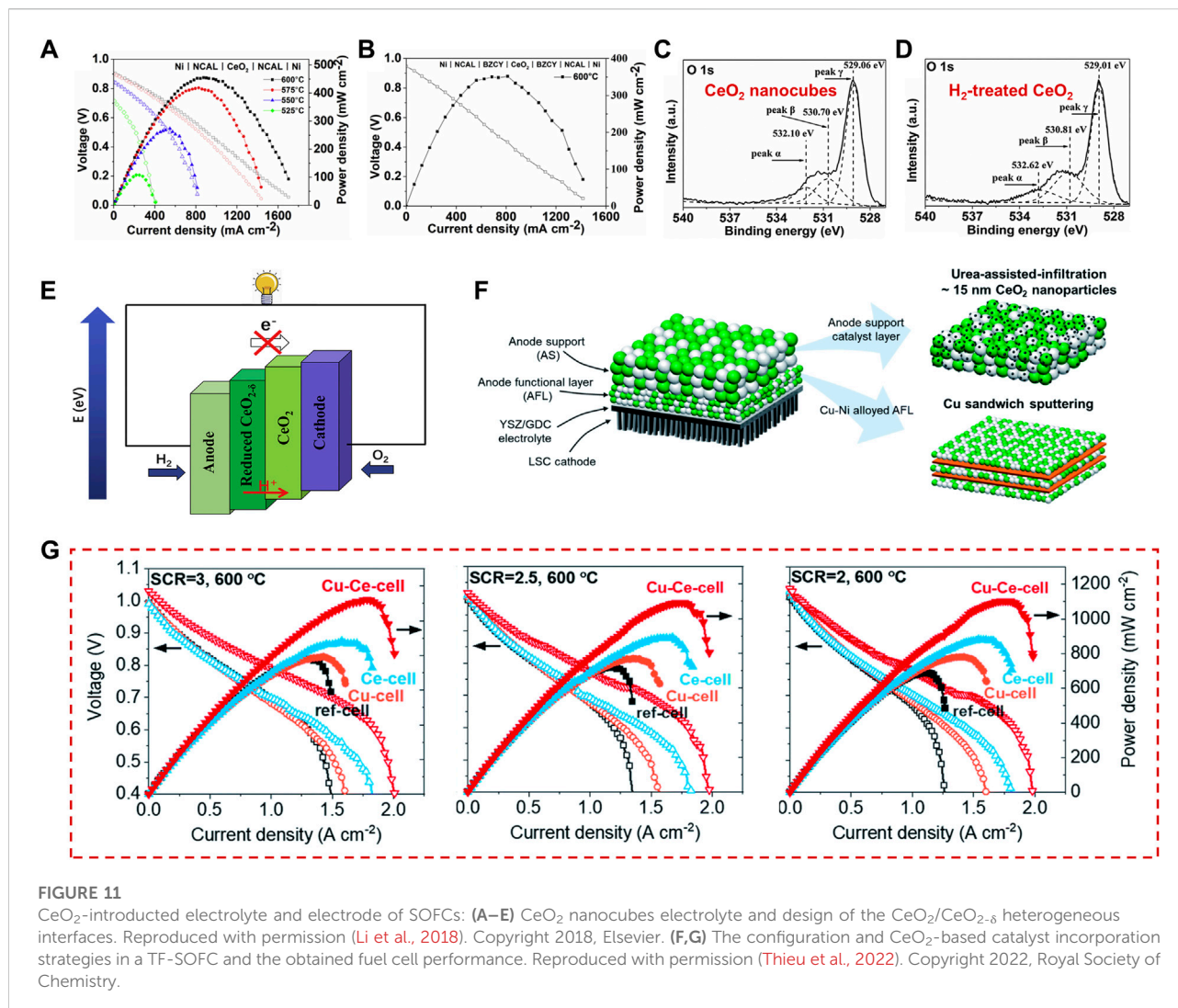### 3.2.2 Proton exchange membrane fuel cells

The proton exchange membrane fuel cell (PEMFC) with considerable power density and energy efficiency is one of the most promising candidates for renewable and sustainable energy conversion devices because of its zero CO$_2$ emissions, which is widely used as clean energy conversion devices, especially in vehicles and some mobile systems powering. The configuration of PEMFC can be seen in Figure 10A. During the PEMFC working, H$_2$ gas at the anode is oxidized to release protons and electrons, then the released electrons generate electricity at the external circuit. The protons, i.e., hydrogen ions, migrate through the polymer electrolyte (proton exchange membrane) to recombine with electrons and oxygen and produce water at the cathode (Majlan et al., 2018). Therein, the catalyst is necessary for accelerating the oxidation of hydrogen gas and reducing oxygen gas to water. The high cost owing to the use of noble metals as

catalysts slows the development and commercialization of PEMFCs (Tasic et al., 2009). Therefore, reducing the use of noble metal catalysts and gradually replacing noble metal with a non-noble metal in the anode, is an important direction for the development of PEMFCs.

Fiala and co-workers have reported a novel carbon supported anode catalysts consisting of thin films of ceria with low Pt loadings (Pt^{2+}-CeO$_2$) (Fiala et al., 2016). They pointed out that the presence of Pt^{2+} is important for enhancing electrocatalytic activity and the stability of Pt^{2+} on ceria enabled the resistance to hydrogenation reduction. Meanwhile, the formation of such stable surface complexes benefits to prevent the degradation of the composite catalysts and improve the durability. To clear the reasonable amount of Pt in the Pt-doped CeO$_2$ thin film, the chemical state of Pt was related to the Pt content in the ceria film *via* XPS spectra analysis (Figure 10B). They found that low Pt loadings would give such thin film with Pt species in the +2 state only. However, the excess Pt content would give rise to the appearance of metallic Pt, indicating that the sites for the accommodation of Pt^{2+} in square-planar coordination of O atoms were limited. Remarkably, only small amounts of surface Pt^{2+} can realize a high power density value of 0.41W cm^{-2}, which is comparable to the reference commercial catalysts (Figure 10C). When calculated into specific power, this value was 205 kW·g$_{(Pt)}^{-1}$, much higher than that of reference commercial catalysts (0.22 kW·g$_{(Pt)}^{1}$).

3.2.3 Solid oxide fuel cells

Solid oxide fuel cells (SOFCs) are a form of fuel cell that consists of a porous anode and cathode separated by a highly dense electrolyte [such as yttria-stabilized zirconia (YSZ) or gadolinium doped ceria (GDC)]. Because of their considerable electrical efficiency, the possibility of using a variety of fuels, and the benign environmental impact, SOFCs have attracted

FIGURE 11
CeO$_2$-introducted electrolyte and electrode of SOFCs: **(A–E)** CeO$_2$ nanocubes electrolyte and design of the CeO$_2$/CeO$_{2-\delta}$ heterogeneous interfaces. Reproduced with permission (Li et al., 2018). Copyright 2018, Elsevier. **(F,G)** The configuration and CeO$_2$-based catalyst incorporation strategies in a TF-SOFC and the obtained fuel cell performance. Reproduced with permission (Thieu et al., 2022). Copyright 2022, Royal Society of Chemistry.

wide attention (Menzler et al., 2010). Although many key materials for SOFCs have been developed in the last decades, there are still great challenges in improving durability and decreasing cost (Suntivich et al., 2011). Currently, the researches on SOFCs materials mainly focus on the optimization of anode, cathode and electrolyte. As CeO$_2$ can be not only used as catalysts or catalyst supports in electrodes, but also explored as electrolytes with improved ionic conductivity, it was widely used in SOFCs (Mogensen, 1994). For example, non-doping CeO$_2$ nanocubes were used as an electrolyte in advanced fuel cells and exhibited outstanding performance (Li et al., 2018). In the case of the CeO$_2$-coated NaFeO$_2$ proton-conducting electrolyte, the addition of the CeO$_2$ shell layer not only increased the number of oxygen vacancies for proton transport but also introduced heterointerface for enhancing ionic boundary conductivity (Xing et al., 2021). This section summarizes the

applications of CeO$_2$ used as an electrolyte and electrode component in SOFCs.

When used as an electrolyte, ceria is generally doped with other trivalent element (or less commonly bivalent) to realize a significant improvement of the ionic conductivity. Common dopants include calcium (Sudarsan and Moorthy, 2019), yttrium, samarium (Bhabu et al., 2016), and gadolinium (Khan et al., 2019). In comparison to the single-phase electrolytes, doping increases the oxygen vacancy concentration, which dictates ionic conduction. Li and co-workers have synthesized CeO$_2$ nanocube with exposed the (100) and (110) active crystal facets and obtained an excellent power density of 406 mW·cm^{-2} at 600 C by using the un-doped CeO$_2$ nanocubes as an electrolyte for advanced fuel cell (Figures 11A,B) (Li et al., 2018). To reveal the origin of the excellent fuel cell performance, they calculated the number of oxygen vacancies of the H$_2$-treated CeO$_2$ (CeO$_{2-\delta}$) and CeO$_2$ nanocubes from the
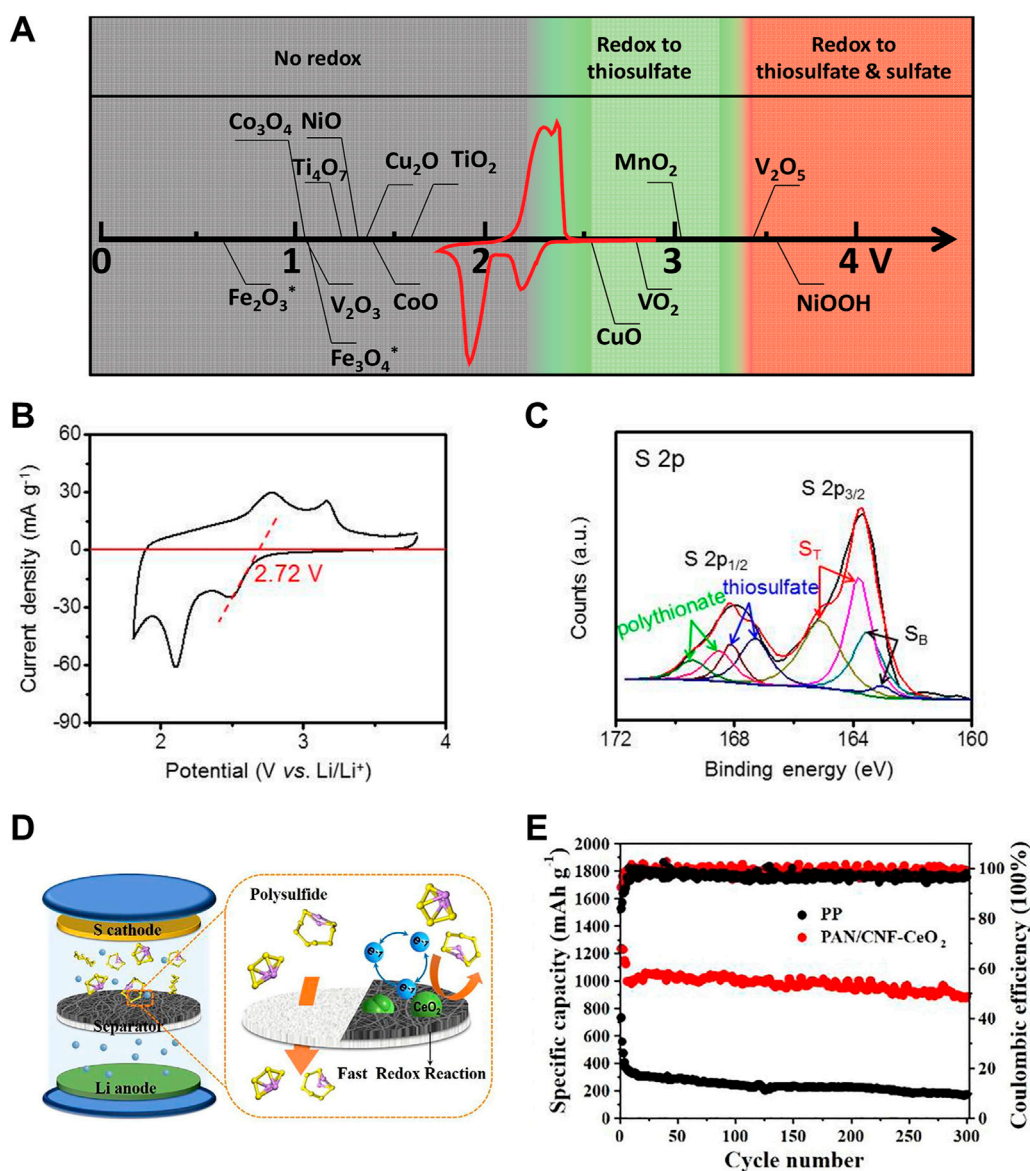
FIGURE 12
Applications of CeO_2 in Li-S batteries: **(A)** Chemical reactivity of different metal oxides with LiPSs as a function of redox potential versus Li/Li⁺, superimposed with a typical Li-S cyclic voltammetry curve. Reproduced with permission (Liang et al., 2016). Copyright 2016, Wiley Online Library. **(B)** Chemical reactivity of CeO_2. **(C)** High-resolution XPS spectrum at S $2p$ region after the adsorption test of Li_2S_4 with CeO_2/MMNC. Reproduced with permission (Ma et al., 2017). Copyright 2017, American Chemical Society. **(D,E)** Catalytic mechanism and performance of a Li-S battery with PAN/CNF-CeO_2 interlayer. Reproduced with permission (Zhang J. et al., 2020). Copyright 2020, Elsevier.

XPS spectra, which showed an increased amount of oxygen vacancies and a higher Ce^{3+} percentage for the H_2-treated CeO_2 (Figures 11C,D). Moreover, a lower activation energy of 0.63 eV was found for CeO_2 nanocubes-introduced fuel cells, which is superior to that of YSZ (0.91 eV) (Strlckler and Carlson, 1965) and other oxide ion conductors (Rupp and Gauckler, 2006). As confirmed by previous studies, major proton conducting mechanism in oxides is conducted by oxygen vacancies, thus proton conduction is highly related to the

concentration of oxygen vacancies. Therefore, they inferred that the surface of the defective CeO_2 nanocube can enhance proton transport through its abundant oxygen vacancies and its conductivity is governed by interfacial ionic transportation. As shown in Figure 11E, the semiconducting energy band differences between the reduced CeO_2 ($CeO_{2-\delta}$) at the anode and oxidized CeO_2 at the cathode side form the double layer device, which can achieve effective charge separation and avoid the device short-circuiting. This work demonstrated the CeO_2/

$CeO_{2-\delta}$ heterogeneous interfaces with a high ionic conductive path conductor and provided a well electrolyte choice for advanced SOFCs, which widen the selecting range of various electrolyte candidates. Besides, ceria is often combined with other components, for example, transition metal layered oxides (TMLOs), carbonates, oxides (Raza et al., 2011), hydroxides (Hu et al., 2006), sulfates (Liu et al., 2005), and halides (Zhu et al., 2001), etc., to create a better low-temperature SOFCs (LT-SOFCs) (Wang et al., 2008; Benamira et al., 2011; Fan et al., 2013). Xing and co-workers reported the CeO_2 coated $NaFeO_2$ as an electrolyte material for LT-SOFC (Xing et al., 2021). They found that the CeO_2 shell layer introduces more oxygen vacancies for proton transfer in the obtained electrolyte material. Meanwhile, the heterointerface is in favor of the O^{2-} grain boundary conductivity. As a result, both the open-circuit voltage (OCV) and the power output of the fuel cells were greatly improved. The fuel cell delivered an admirable power output of 727 mW·cm^{-2} at 550°C by using the core cell $NaFeO_2$-CeO_2 composites as an electrolyte.

Another widely explored field in SOFCs developments is ceria-based composite cathodes and anodes, such as Pd@CeO_2 (Adijanto et al., 2013), Ru-CeO_2 (Zhan and Barnett, 2005), Ni-CeO_2 (Lee et al., 2013), and so on. As a high cost of the noble-metal catalysts, Thieu and co-workers prepared the catalyst-modified cells with Cu and CeO_2 (Cu-Ce-cell), in which Cu was inserted directly near the electrolyte-anode interface and CeO_2 was incorporated into the anode support to effectively facilitate thermochemical reforming reactions (Figure 11F) (Thieu et al., 2022). As shown in Figure 11G, Cu-Ce-cell exhibited a record high performance with a peak power density of 1,120 mW·cm^{-2} at 600°C. The peak power densities of Cu-Ce-cell did not significantly change with the different steam-to-carbon ratios (SCRs). Furthermore, Cu-Ce-cell showed long-term performances with only slight voltage degradation of ~2.76% over 250 h under a constant current load of 0.15 A·cm^{-2} by using butane fuel with an SCR of 3 at 600°C.

3.2.4 Sulfur conversion reaction in lithium-sulfur batteries

Lithium-sulfur (Li-S) batteries are regarded as a promising energy storage system for new generation portable electronic devices and electric vehicles due to their high theoretical energy density (2,600 Wh·kg^{-1}) and specific capacity (1,675 mAh·g^{-1}) as well as the low cost, natural abundance, and environmentally friendly nature of sulfur (Urbonaite et al., 2015). However, the insulating property of sulfur and its discharge products leads to limited reaction kinetics during the redox processes, which results in low utilization of sulfur and insufficient practical specific capacity. Furthermore, in the multistep sulfur reduction reaction, the conversion of the soluble lithium polysulfide intermediates (LiPSs) into insoluble Li_2S_2/Li_2S has a much higher apparent activation energy, which will lead to the accumulation of polysulfides in the liquid electrolyte, a

continuous loss of active sulfur from the cathode and the final battery failure. Therefore, introducing electrocatalysts in Li-S cells towards fast sulfur conversions is of great significance for decreasing the activation energy of the precipitation of Li_2S_2/Li_2S solids and improving Li-S battery performances (Liu et al., 2021). Metal oxides, sulfides, nitrides, phosphides, and their heterostructures have been screened in a large number of studies (Yuan et al., 2016; Sun et al., 2017; Zhang M. et al., 2020; Hua et al., 2021; Xia et al., 2021). Liang et al. (2016) have pointed out that only materials with redox potentials in a targeted window can react with polysulfides to form active surface-bound polythionate species. And they deemed that the formed active surface-bound polythionate species have direct correlation with the superior Li-S cell performance (Figure 12A). These metal oxides with redox potentials between 2.4 and 3.05 V (such as VO_2 and CuO) possess a window that lies just above the redox voltage of soluble polysulfides and thus promotes polythionate formation. A higher redox potential will lead to excessive oxidization of polysulfides, and a lower one shows no redox reaction with polysulfides. CeO_2 is a polar metal oxide that can chemically adsorb the sulfur species and boost redox reaction through catalysis. Meanwhile, CeO_2 nanocrystals possess a proper redox potential of 2.72 V vs. Li/Li$^+$, which is higher than that of polysulfides (2.10 V vs. Li/Li$^+$). Accordingly, the CeO_2 nanocrystals might oxidize the intermediate polysulfides to thiosulfates and polythionates via the surface redox chemistry (Figures 12B,C) (Ma et al., 2017). Therefore, many CeO_2-based nanostructures have been reported to be used as electrocatalysts to promote Li-S cell performance.

Ma and co-workers demonstrate an advanced sulfur host material prepared by implanting CeO_2 nanocrystals homogeneously into bimodal micromesoporous nitrogen-rich carbon nanospheres (CeO_2/MMNC) (Ma et al., 2017). This hybrid with high conductivity and abundant hierarchical pore structures can effectively store and capture sulfur species. Meanwhile, the CeO_2 can promote the chemical redox reactions of polysulfides, thus significantly enhancing their retentions upon cycling. As a result, CeO_2/MMNC-S cathodes showed the excellent capacity and rate performance, as well as an ultralong cycle life. Specifically, the cathode with a sulfur mass loading of 1.4 mg·cm^{-2} realized the reversible capacities of 1,066 mAh·g^{-1} at 0.2 C after 200 cycles and 836 mAh·g^{-1} at 1.0 C after 500 cycles, and a high cycle stability of 721 mAh·g^{-1} at 2.0 C after 1,000 cycles with a low capacity decay of 0.024% per cycle. Besides carbon nanospheres, other carbon materials, such as carbon nanotubes (CNTs) and graphene, are often used as supports to disperse the active CeO_2 nanocrystal (Ma et al., 2017). Yuan et al. have designed a three-dimension porous conductive network of CeO_2-webbed carbon nanotubes (CeO_2@CNT) to provide fast electron paths and achieve a good rate capability in the Li-S batteries (Xiao et al., 2018). In order to increase the sulfur utilization, CNT particles with high tap density were applied to realize a uniform melt-diffusion of

sulfur by Gueon and co-authors. They further demonstrated microdomain sulfur by coating the CeO_2 nanoparticles in a CNT with an open pore structure. The open pore structure of CeO_2/CNTP and the microdomain sulfur enabled fast kinetics in the redox reaction of sulfur, and therefore achieving excellent cycling stability of only 0.044% per cycle for 300 cycles at 2 C and a high capacity of 5.6 mAh·cm^{-2} even at high sulfur loading (Gueon et al., 2020). In addition, CeO_2 was used as cathode materials alone by constructing phosphorus-modulated porous CeO_2 (P-CeO_2) as reported by Tao et al. (2022). The P-CeO_2 cathode showed a better oxidation-reduction kinetics of LiPSs and a faster Li$^+$ diffusion rate in comparison to that of bare CeO_2. Meanwhile, they have confirmed that the P-CeO_2 cathode presented stronger adsorption of Li_2S_6, higher redox peak current, and earlier precipitation of Li_2S in comparison to the bare CeO_2. Therefore, introducing P resulted in an improved initial capacity of 1,027 mA·h·g^{-1} (bare CeO_2: 895.7 mA·h·g^{-1}) at 0.2 C.

Apart from the sulfur host, CeO_2 has also been used in the separator modification. Generally, the soluble polysulfides can be immobilized in the cathode side by the multifunctional modified interlayer. Cheng et al. have designed a multifunctional separator modified by CeO_2 decorated graphene (CeO_2@G) to accelerate polysulfide redox reaction and immobilize polysulfides by strong chemisorption (Cheng et al., 2021). Zhang and co-authors fabricated a functional bilayer separator based on 0D (CeO_2 nanocrystals)/1D (carbon nanofibers) composite mats (PAN/CNF-CeO_2) (Zhang J. et al., 2020). By integrating the advantages of highly conductive carbon nanofibers and electrocatalytically active CeO_2 nanocrystals, the Li-S batteries with the obtained PAN/CNF-CeO_2 separators showed high S utilization, excellent thermal stability, superior rate performance and enhanced cycling stability (Figure 12D). Specifically, the Li-S cell exhibited an initial reversible capacity of 1,359 mAh·g^{-1} at 0.2 C and a low capacity decay rate of 0.04% per cycle at 0.5 C over 300 cycles (Figure 12E).

4 Summary and outlook

In this review, we introduce the electronic properties and defects engineering of CeO_2-based nanostructures to understand the relationship between catalytic performance and inherent properties. The typical catalytic applications in energy conversion and storage of CeO_2-based nanostructures have also been demonstrated. Therein, the mechanisms and key component developments of several photocatalytic reactions and representative energy storage cells have also been summarized. With great progress being made in the synthesis of CeO_2-based nanostructures, there are fascinating new opportunities and challenges for materials scientists. The

understanding of CeO_2 materials has evolved in the last decades from inert supports through cocatalysts and to the catalyst itself (Montini et al., 2016). The development of nanotechnology made it possible to acquire well-controlled nanomaterials in terms of size and morphology, which has improved our understanding on the catalytic performance optimization of CeO_2-based nanocatalysts. Moreover, there are many theoretical calculations for providing a guideline on the rational design of highly reactive CeO_2-based catalysts. In applications for energy storage and conversion through photocatalysis and electrocatalysis, CeO_2 is frequently utilized as a catalyst or a crucial component of catalysts. In conclusion, CeO_2 is an extremely adaptable and durable catalytic material with surface acid-base characteristics and a structure that can be finely modified by element doping and introducing other compounds. Although many of the studies on CeO_2-based nanostructures reported so far have shown considerable progress in its catalytic application, more attentions need to be paid to the synthesis, characterization approaches and practical uses. For example, the precise synthesis methods still need to be paid attention to realize the controllable defects concentration and selectively exposed crystal facets. Introducing other elements or components in CeO_2 to construct composites, heterojunctions and modifications is commonly, which can regulate the electronic structure of the catalyst or optimize the properties of CeO_2. However, it is also quite necessary to prepare specifically nanostructured oriented ceria-based systems (for example porous structures, core-shell structures, hollow structures, surface acidity, and basicity of Lewis sites, etc.) to realize desired catalytic performance, in addition to above mentioned. Precise synthesis is not only critical for enhancing catalytic performance but also for providing valuable references for our research on catalytic mechanisms. At present, controlled generation of oxygen vacancies and cerium defects is challenging and needs more experimental explorations. The long-term stability of the CeO_2 nanostructures under extreme conditions and reaction conditions is of potential concern. Especially, oxygen vacancy stabilization is a noteworthy issue. Oxygen vacancies are generally considered as the important active sites, therefore ensuring the similar densities of oxygen vacancies on CeO_2-based catalysts after cycling test is one of key metrics. The relationship between material inherent properties and catalytic performances should be understood by a simple and experimentally measurable descriptor instead of mere theory calculations. Further basic understanding of burgeoning novel materials and direct confirmation of the effect on catalytic efficiency are conductive to develop a strong understanding of structure-activity interlinkage and guide researchers to design and synthesize extraordinary CeO_2 nanostructures.

Author contributions

XW wrote original manuscripts. TS revised the manuscript and is responsible for this work. All authors discussed and approved the final manuscript version to be submitted.

Funding

Conflict of interest

The authors declare that the research was conducted in the absence of any commercial or financial relationships that could be construed as a potential conflict of interest.

Publisher's note

All claims expressed in this article are solely those of the authors and do not necessarily represent those of their affiliated organizations, or those of the publisher, the editors and the reviewers. Any product that may be evaluated in this article, or claim that may be made by its manufacturer, is not guaranteed or endorsed by the publisher.

References

Adijanto, L., Sampath, A., Yu, A. S., Cargnello, M., Fornasiero, P., Gorte, R. J., et al. (2013). Synthesis and stability of Pd@CeO$_2$ core-shell catalyst films in solid oxide fuel cell anodes. *ACS Catal.* 3 (8), 1801–1809. doi:10.1021/cs4004112

Amoresi, R. A. C., Oliveira, R. C., Marana, N. L., de Almeida, P. B., Prata, P. S., Zaghete, M. A., et al. (2019). CeO$_2$ nanoparticle morphologies and their corresponding crystalline planes for the photocatalytic degradation of organic pollutants. *ACS Appl. Nano Mat.* 2 (10), 6513–6526. doi:10.1021/acsanm.9b01452

Arul, N. S., Mangalaraj, D., and Han, J. I. (2015). Enhanced photocatalytic property of self-assembled Fe-doped CeO$_2$ hierarchical nanostructures. *Mat. Lett.* 145, 189–192. doi:10.1016/j.matlet.2015.01.075

Benamira, M., Ringuede, A., Albin, V., Vannier, R. N., Hildebrandt, L., Lagergren, C., et al. (2011). Gadolinia-doped ceria mixed with alkali carbonates for solid oxide fuel cell applications: I. A thermal, structural and morphological insight. *J. Power Sources* 196 (13), 5546–5554. doi:10.1016/j.jpowsour.2011.02.004

Bhabu, K. A., Theerthagiri, J., Madhavan, J., Balu, T., Muralidharan, G., and Rajasekaran, T. R. (2016). Cubic fluorite phase of samarium doped cerium oxide (CeO$_2$)(0.96)Sm-0.04 for solid oxide fuel cell electrolyte. *J. Mat. Sci. Mat. Electron.* 27 (2), 1566–1573. doi:10.1007/s10854-015-3925-z

Bian, H., Ji, Y., Yan, J., Li, P., Li, L., Li, Y., et al. (2018). *In situ* synthesis of few-layered g-C$_3$N$_4$ with vertically aligned MoS$_2$ loading for boosting solar-to-hydrogen generation. *Small* 14 (3), 1703003. doi:10.1002/smll.201703003

Cai, R., Ju, M., Chen, J., Ren, J., Yu, J., Long, X., et al. (2021). Recent advances in surface/interface engineering of noble-metal free catalysts for energy conversion reactions. *Mat. Chem. Front.* 5 (9), 3576–3592. doi:10.1039/d1qm00161b

Cai, W., Shi, Y., Zhao, Y., Chen, M., Zhong, Q., and Bu, Y. (2018). The solvent-driven formation of multi-morphological Ag-CeO$_2$ plasmonic photocatalysts with enhanced visible-light photocatalytic reduction of CO$_2$. *RSC Adv.* 8 (71), 40731–40739. doi:10.1039/c8ra08938h

Cao, Z., Ran, G., Wang, Z., Li, Y., Wu, X., Wu, L., et al. (2022). *In-situ* TEM study on the evolution of dislocation loops and bubbles in CeO$_2$ during Kr$^+$ single-beam and Kr$^+$-H$_2^+$ dual-beam synergetic irradiation. *J. Mat. Sci. Technol.* 123, 49–59. doi:10.1016/j.jmst.2022.01.021

Chen, B., Ma, Y., Ding, L., Xu, L., Wu, Z., Yuan, Q., et al. (2013). Reactivity of hydroxyls and water on a CeO$_2$(111) thin film surface: The role of oxygen vacancy. *J. Phys. Chem. C* 117 (11), 5800–5810. doi:10.1021/jp312406f

Cheng, P., Guo, P., Sun, K., Zhao, Y., Liu, D., and He, D. (2021). CeO$_2$ decorated graphene as separator modification material for capture and boost conversion of polysulfide in lithium-sulfur batteries. *J. Memb. Sci.* 619, 118780. doi:10.1016/j.memsci.2020.118780

Corma, A., Atienzar, P., García, H., and Chane-Ching, J. Y. (2004). Hierarchically mesostructured doped CeO$_2$ with potential for solar-cell use. *Nat. Mat.* 3 (6), 394–397. doi:10.1038/nmat1129

Dai, W., Hu, X., Wang, T., Xiong, W., Luo, X., and Zou, J. (2018a). Hierarchical CeO$_2$/Bi$_2$MoO$_6$ heterostructured nanocomposites for photoreduction of CO$_2$ into hydrocarbons under visible light irradiation. *Appl. Surf. Sci.* 434, 481–491. doi:10.1016/j.apsusc.2017.10.207

Dai, Y., Li, C., Shen, Y., Lim, T., Xu, J., Li, Y., et al. (2018b). Light-tuned selective photosynthesis of azo- and azoxy-aromatics using graphitic C$_3$N$_4$. *Nat. Commun.* 9, 60. doi:10.1038/s41467-017-02527-8

Danilovic, N., Subbaraman, R., Chang, K. C., Chang, S. H., Kang, Y., Snyder, J., et al. (2014). Using surface segregation to design stable Ru-Ir oxides for the oxygen evolution reaction in acidic environments. *Angew. Chem. Int. Ed.* 53 (51), 14016–14021. doi:10.1002/anie.201406455

Dong, B., Li, L., Dong, Z., Xu, R., and Wu, Y. (2018). Fabrication of CeO$_2$ nanorods for enhanced solar photocatalysts. *Int. J. Hydrogen Energy* 43 (10), 5275–5282. doi:10.1016/j.ijhydene.2017.10.061

Dung Van, D., Nguyen, T. T. D., Uthirakumar, P., Cho, Y.-H., Kim, G.-C., Yang, J.-K., et al. (2021). Insightful understanding of hot-carrier generation and transfer in plasmonic Au@CeO$_2$ core-shell photocatalysts for light-driven hydrogen evolution improvement. *Appl. Catal. B Environ.* 286, 119947. doi:10.1016/j.apcatb.2021.119947

Esch, F., Fabris, S., Zhou, L., Montini, T., Africh, C., Fornasiero, P., et al. (2005). Electron localization determines defect formation on ceria substrates. *Science* 309, 752–755. doi:10.1126/science.1111568

Fan, L., Zhang, H., Chen, M., Wang, C., Wang, H., Singh, M., et al. (2013). Electrochemical study of lithiated transition metal oxide composite as symmetrical electrode for low temperature ceramic fuel cells. *Int. J. Hydrogen Energy* 38 (26), 11398–11405. doi:10.1016/j.ijhydene.2013.06.050

Fiala, R., Figueroba, A., Bruix, A., Vaclavu, M., Rednyk, A., Khalakhan, I., et al. (2016). High efficiency of Pt^{2+}-CeO$_2$ novel thin film catalyst as anode for proton exchange membrane fuel cells. *Appl. Catal. B Environ.* 197, 262–270. doi:10.1016/j.apcatb.2016.02.036

Fiorenza, R., Bellardita, M., Balsamo, S. A., Spitaleri, L., Gulino, A., Condorelli, M., et al. (2022). A solar photothermocatalytic approach for the CO$_2$ conversion: Investigation of different synergisms in CoO-CuO/brookite TiO$_2$-CeO$_2$ catalysts. *Chem. Eng. J.* 428, 131249. doi:10.1016/j.cej.2021.131249

Fujimori, A. (1984). Comment on "spectroscopic evidence for localized and extended *f*-symmetry states in CeO$_2$. *Phys. Rev. Lett.* 53 (26), 2518. doi:10.1103/PhysRevLett.53.2518

Fukui, K.-i., Namai, Y., and Iwasawa, Y. (2002). Imaging of surface oxygen atoms and their defect structures on CeO$_2$(1 1 1) by noncontact atomic force microscopy. *Appl. Surf. Sci.* 188 (3), 252–256. doi:10.1016/S0169-4332(01)00917-5

Ganduglia-Pirovano, M. V., Hofmann, A., and Sauer, J. (2007). Oxygen vacancies in transition metal and rare Earth oxides: Current state of understanding and remaining challenges. *Surf. Sci. Rep.* 62 (6), 219–270. doi:10.1016/j.surfrep.2007.03.002

Gao, D., Zhang, Y., Zhou, Z., Cai, F., Zhao, X., Huang, W., et al. (2017). Enhancing CO$_2$ electroreduction with the metal-oxide interface. *J. Am. Chem. Soc.* 139 (16), 5652–5655. doi:10.1021/jacs.7b00102

Gao, W., Xia, Z., Cao, F., Ho, J. C., Jiang, Z., and Qu, Y. (2018). Comprehensive understanding of the spatial configurations of CeO$_2$ in NiO for the electrocatalytic oxygen evolution reaction: Embedded or surface-loaded. *Adv. Funct. Mat.* 28 (11), 1706056. doi:10.1002/adfm.201706056

Gennard, S., Corà, F., and Catlow, C. R. A. (1999). Comparison of the bulk and surface properties of ceria and zirconia by *ab initio* investigations. *J. Phys. Chem. B* 103 (46), 10158–10170. doi:10.1021/jp9913923

Gou, W., Xia, Z., Tan, X., Xue, Q., Ye, F., Dai, S., et al. (2022). Highly active and stable amorphous IrOx/CeO2 nanowires for acidic oxygen evolution. *Nano Energy* 104, 107960. doi:10.1016/j.nanoen.2022.107960

Gueon, D., Yoon, J., Hwang, J. T., and Moon, J. H. (2020). Microdomain sulfur-impregnated CeO2-coated CNT particles for high-performance Li-S batteries. *Chem. Eng. J.* 390, 124548. doi:10.1016/j.cej.2020.124548

Hamidah Abdullah, N. A. I., Yaakob, Z., Khan, M. R., and Rahim, S. A. (2017). CeO2-TiO2 for photoreduction of CO2 to methanol under visible light: Effect of ceria loading. *Malays. J. Anal. Sci.* 21, 166–172. doi:10.175676/mjas-2017-2101-19

Han, Q., Wu, C., Jiao, H., Xu, R., Wang, Y., Xie, J., et al. (2021). Rational design of high-concentration Ti³⁺ in porous carbon-doped TiO2 nanosheets for efficient photocatalytic ammonia synthesis. *Adv. Mat.* 33 (9), 2008180. doi:10.1002/adma.202008180

Hansen, H. A., and Wolverton, C. (2014). Kinetics and thermodynamics of H2O dissociation on reduced CeO2(111). *J. Phys. Chem. C* 118 (47), 27402–27414. doi:10.1021/jp508666c

Hao, J., Zhan, W., Sun, L., Zhuang, G., Wang, X., and Han, X. (2020). Combining N, S-codoped C and CeO2: A unique hinge-like structure for efficient photocatalytic hydrogen evolution. *Inorg. Chem.* 59 (1), 937–942. doi:10.1021/acs.inorgchem.9b03204

He, X., Yi, X., Yin, F., Chen, B., Li, G., and Yin, H. (2019). Less active CeO2 regulating bifunctional oxygen electrocatalytic activity of Co3O4@N-doped carbon for Zn–air batteries. *J. Mat. Chem. A* 7 (12), 6753–6765. doi:10.1039/C9TA00302A

Hezam, A., Namratha, K., Drmosh, Q. A., Ponnamma, D., Wang, J., Prasad, S., et al. (2020). CeO2 nanostructures enriched with oxygen vacancies for photocatalytic CO2 reduction. *ACS Appl. Nano Mat.* 3 (1), 138–148. doi:10.1021/acsanm.9b01833

Hill, S. E., and Catlow, C. R. A. (1993). A Hartree-Fock periodic study of bulk ceria. *J. Phys. Chem. Solids* 54 (4), 411–419. doi:10.1016/0022-3697(93)90322-I

Hojo, H., Mizoguchi, T., Ohta, H., Findlay, S. D., Shibata, N., Yamamoto, T., et al. (2010). Atomic structure of a CeO2 grain boundary: The role of oxygen vacancies. *Nano Lett.* 10 (11), 4668–4672. doi:10.1021/nl1029336

Hojo, H., Tochigi, E., Mizoguchi, T., Ohta, H., Shibata, N., Feng, B., et al. (2011). Atomic structure and strain field of threading dislocations in CeO2 thin films on yttria-stabilized ZrO2. *Appl. Phys. Lett.* 98 (15), 153104. doi:10.1063/1.3575566

Hu, J. G., Tosto, S., Guo, Z. X., and Wang, W. F. (2006). Dual-phase electrolytes for advanced fuel cells. *J. Power Sources* 154 (1), 106–114. doi:10.1016/j.jpowsour.2005.03.225

Hua, W., Li, H., Pei, C., Xia, J., Sun, Y., Zhang, C., et al. (2021). Selective catalysis remedies polysulfide shuttling in lithium-sulfur batteries. *Adv. Mat.* 33 (38), 2101006. doi:10.1002/adma.202101006

Huang, W. (2016). Oxide nanocrystal model catalysts. *Acc. Chem. Res.* 49 (3), 520–527. doi:10.1021/acs.accounts.5b00537

Huang, Z.-Q., Liu, L.-P., Qi, S., Zhang, S., Qu, Y., and Chang, C.-R. (2018). Understanding all-solid frustrated-Lewis-pair sites on CeO2 from theoretical perspectives. *ACS Catal.* 8 (1), 546–554. doi:10.1021/acscatal.7b02732

Ji, P., Zhang, J., Chen, F., and Anpo, M. (2008). Ordered mesoporous CeO2 synthesized by nanocasting from cubic Ia3d mesoporous MCM-48 silica: Formation, characterization and photocatalytic activity. *J. Phys. Chem. C* 112 (46), 17809–17813. doi:10.1021/jp8054087

Khan, I., Tiwari, P. K., and Basu, S. (2019). Development of melt infiltrated gadolinium doped ceria-carbonate composite electrolytes for intermediate temperature solid oxide fuel cells. *Electrochim. Acta* 294, 1–10. doi:10.1016/j.electacta.2018.10.030

Koelling, D. D., Boring, A. M., and Wood, J. H. (1983). The electronic structure of CeO2 and PrO2. *Solid State Commun.* 47 (4), 227–232. doi:10.1016/0038-1098(83)90550-1

Kong, J., Xiang, Z., Li, G., and An, T. (2020). Introduce oxygen vacancies into CeO2 catalyst for enhanced coke resistance during photothermocatalytic oxidation of typical VOCs. *Appl. Catal. B Environ.* 269, 118755. doi:10.1016/j.apcatb.2020.118755

Kumaran, C., Baskaran, I., Sathyaseelan, B., Senthilnathan, K., Manikandan, E., and Sambasivam, S. (2022). Effect of doping of iron on structural, optical and magnetic properties of CeO2 nanoparticles. *Chem. Phys. Lett.* 808, 140110. doi:10.1016/j.cplett.2022.140110

Lai, H., Zeng, X., Song, T., Yin, S., Long, B., Ali, A., et al. (2022). Fast synthesis of porous iron doped CeO2 with oxygen vacancy for effective CO2 photoreduction. *J. Colloid Interface Sci.* 608, 1792–1801. doi:10.1016/j.jcis.2021.10.064

Lee, Y.-H., Sumi, H., Muroyama, H., Matsui, T., and Eguchi, K. (2013). Influence of Ni-oxide anode thickness on performance stability in Internal reforming of methane for solid oxide fuel cells. *J. Electrochem. Soc.* 160 (6), F579–F584. doi:10.1149/2.075306jes

Li, H.-Y., Wang, H.-F., Gong, X.-Q., Guo, Y.-L., Guo, Y., Lu, G., et al. (2009). Multiple configurations of the two excess 4f electrons on defective CeO2(111): Origin and implications. *Phys. Rev. B* 79 (19), 193401. doi:10.1103/PhysRevB.79.193401

Li, J., Xia, Z., Xue, Q., Zhang, M., Zhang, S., Xiao, H., et al. (2021a). Insights into the interfacial Lewis acid-base pairs in CeO2-loaded CoS2 electrocatalysts for alkaline hydrogen evolution. *Small* 17 (39), 2103018. doi:10.1002/smll.202103018

Li, L., Zhu, B., Zhang, J., Yan, C., and Wu, Y. (2018). Electrical properties of nanocube CeO2 in advanced solid oxide fuel cells. *Int. J. Hydrogen Energy* 43 (28), 12909–12916. doi:10.1016/j.ijhydene.2018.05.120

Li, Q., Song, L., Liang, Z., Sun, M., Wu, T., Huang, B., et al. (2021b). A review on CeO(2)-based electrocatalyst and photocatalyst in energy conversion. *Adv. Energy Sustain. Res.* 2 (2), 2000063. doi:10.1002/aesr.202000063

Li, W., Jin, L., Gao, F., Wan, H., Pu, Y., Wei, X., et al. (2021c). Advantageous roles of phosphate decorated octahedral CeO2 {111}/g-C3N4 in boosting photocatalytic CO2 reduction: Charge transfer bridge and Lewis basic site. *Appl. Catal. B Environ.* 294, 120257. doi:10.1016/j.apcatb.2021.120257

Li, Y., and Shen, W. (2014). Morphology-dependent nanocatalysts: Rod-shaped oxides. *Chem. Soc. Rev.* 43 (5), 1543–1574. doi:10.1039/c3cs60296f

Li, Y., Zhang, X., and Zheng, Z. (2022). CeO2 functionalized cobalt layered double hydroxide for efficient catalytic oxygen-evolving reaction. *Small* 18 (17), 2107594. doi:10.1002/smll.202107594

Li, Z., Zhang, X., Kang, Y., Yu, C. C., Wen, Y., Hu, M., et al. (2021d). Interface engineering of Co-LDH@MOF heterojunction in highly stable and efficient oxygen evolution reaction. *Adv. Sci.* 8 (2), 2002631. doi:10.1002/advs.202002631

Liang, M., Borjigin, T., Zhang, Y., Liu, B., Liu, H., and Guo, H. (2019). Controlled assemble of hollow heterostructured g-C3N4@CeO2 with rich oxygen vacancies for enhanced photocatalytic CO2 reduction. *Appl. Catal. B Environ.* 243, 566–575. doi:10.1016/j.apcatb.2018.11.010

Liang, X., Kwok, C. Y., Lodi-Marzano, F., Pang, Q., Cuisinier, M., Huang, H., et al. (2016). Tuning transition metal oxide-sulfur interactions for long life lithium sulfur batteries: The "goldilocks" principle. *Adv. Energy Mat.* 6 (6), 1501636. doi:10.1002/aenm.201501636

Lin, Y., Wu, Z., Wen, J., Poeppelmeier, K. R., and Marks, L. D. (2014). Imaging the atomic surface structures of CeO2 nanoparticles. *Nano Lett.* 14 (1), 191–196. doi:10.1021/nl403713b

Liu, N., Ma, H., Wang, L., Zhao, Y., Bakenov, Z., and Wang, X. (2021). Dealloying-derived nanoporous deficient titanium oxide as high-performance bifunctional sulfur host-catalysis material in lithium-sulfur battery. *J. Mat. Sci. Technol.* 84, 124–132. doi:10.1016/j.jmst.2020.11.073

Liu, X. R., Zhu, B., Xu, J. R., Sun, J. C., and Mao, Z. Q. (2005). Sulphate ceria composite ceramics for energy environmental Co-generation technology. *Key Eng. Mat.* 280-283, 425–430. doi:10.4028/www.scientific.net/KEM.280-283.425

Lu, X., Zhai, T., Cui, H., Shi, J., Xie, S., Huang, Y., et al. (2011). Redox cycles promoting photocatalytic hydrogen evolution of CeO2 nanorods. *J. Mat. Chem.* 21 (15), 5569–5572. doi:10.1039/C0JM04466K

Ma, L., Chen, R., Zhu, G., Hu, Y., Wang, Y., Chen, T., et al. (2017). Cerium oxide nanocrystal embedded bimodal micromesoporous nitrogen-rich carbon nanospheres as effective sulfur host for lithium-sulfur batteries. *ACS Nano* 11 (7), 7274–7283. doi:10.1021/acsnano.7b03227

Ma, Y., Zhang, S., Chang, C.-R., Huang, Z.-Q., Ho, J. C., and Qu, Y. (2018). Semi-solid and solid frustrated Lewis pair catalysts. *Chem. Soc. Rev.* 47 (15), 5541–5553. doi:10.1039/C7CS00691H

Majlan, E. H., Rohendi, D., Daud, W. R. W., Husaini, T., and Haque, M. A. (2018). Electrode for proton exchange membrane fuel cells: A review. *Renew. Sustain. Energy Rev.* 89, 117–134. doi:10.1016/j.rser.2018.03.007

Marabelli, F., and Wachter, P. (1987). Covalent insulator CeO2: Optical reflectivity measurements. *Phys. Rev. B* 36 (2), 1238–1243. doi:10.1103/PhysRevB.36.1238

Melchionna, M., and Fornasiero, P. (2014). The role of ceria-based nanostructured materials in energy applications. *Mat. TodayKidlingt.* 17 (7), 349–357. doi:10.1016/j.mattod.2014.05.005

Menzler, N. H., Tietz, F., Uhlenbruck, S., Buchkremer, H. P., and Stoever, D. (2010). Materials and manufacturing technologies for solid oxide fuel cells. *J. Mat. Sci.* 45 (12), 3109–3135. doi:10.1007/s10853-010-4279-9

Mo, Z., Kolychev, E. L., Rit, A., Campos, J., Niu, H., and Aldridge, S. (2015). Facile reversibility by design: Tuning small molecule capture and activation by single

component frustrated Lewis pairs. *J. Am. Chem. Soc.* 137 (38), 12227–12230. doi:10.1021/jacs.5b08614

Mogensen, M., Lindegaard, T., Hansen, U. R., and Mogensen, G. (1994). Physical properties of mixed conductor solid oxide fuel cell anodes of doped CeO_2. *J. Electrochem. Soc.* 141, 2122–2128. doi:10.1149/1.2055072

Montini, T., Melchionna, M., Monai, M., and Fornasiero, P. (2016). Fundamentals and catalytic applications of CeO_2-based materials. *Chem. Rev.* 116 (10), 5987–6041. doi:10.1021/acs.chemrev.5b00603

Muhammad, A., Tahir, M., Al-Shahrani, S. S., Ali, A. M., and Rather, S. U. (2020). Template free synthesis of graphitic carbon nitride nanotubes mediated by lanthanum (La/g-CNT) for selective photocatalytic CO_2 reduction via dry reforming of methane (DRM) to fuels. *Appl. Surf. Sci.* 504, 144177. doi:10.1016/j.apsusc.2019.144177

Nolan, M., Parker, S. C., and Watson, G. W. (2005). The electronic structure of oxygen vacancy defects at the low index surfaces of ceria. *Surf. Sci.* 595 (1), 223–232. doi:10.1016/j.susc.2005.08.015

Prajapati, P. K., Malik, A., Nandal, N., Pandita, S., Singh, R., Bhandari, S., et al. (2022). Morphology controlled Fe and Ni-doped CeO_2 nanorods as an excellent heterojunction photocatalyst for CO_2 reduction. *Appl. Surf. Sci.* 588, 152912. doi:10.1016/j.apsusc.2022.152912

Primo, A., Marino, T., Corma, A., Molinari, R., and Garcia, H. (2012). Efficient visible-light photocatalytic water splitting by minute amounts of gold supported on nanoparticulate CeO_2 obtained by a biopolymer templating method. *J. Am. Chem. Soc.* 134 (3), 1892. doi:10.1021/ja211206v

Qiu, B., Wang, C., Zhang, N., Cai, L., Xiong, Y., and Chai, Y. (2019). CeO_2-induced interfacial Co^{2+} octahedral sites and oxygen vacancies for water oxidation. *ACS Catal.* 9 (7), 6484–6490. doi:10.1021/acscatal.9b01819

Raza, R., Abbas, G., Imran, S. K., Patel, I., and Zhu, B. (2011). GDC-Y_2O_3 oxide based two phase nanocomposite electrolyte. *J. Fuel Cell. Sci. Technol.* 8 (4). doi:10.1115/1.4003634

Rupp, J. L. M., and Gauckler, L. J. (2006). Microstructures and electrical conductivity of nanocrystalline ceria-based thin films. *Solid State Ionics* 177 (26-32), 2513–2518. doi:10.1016/j.ssi.2006.07.033

Shea, J. J. (2020). Your successful project management career [Book review]. *IEEE Electr. Insul. Mag.* 36 (5), 57. doi:10.1109/mei.2005.1412235

Shen, Z., Xia, Q., Li, Y., Yin, C., Ge, Z., Li, X., et al. (2020). Adsorption-enhanced nitrogen-doped mesoporous CeO_2 as an efficient visible-light-driven catalyst for CO_2 photoreduction. *J. CO2 Util.* 39, 101176. doi:10.1016/j.jcou.2020.101176

Skorodumova, N. V., Ahuja, R., Simak, S. I., Abrikosov, I. A., Johansson, B., and Lundqvist, B. I. (2001). Electronic, bonding, and optical properties ofCeO2andCe2O3from first principles. *Phys. Rev. B* 64 (11), 115108. doi:10.1103/PhysRevB.64.115108

Spezzati, G., Benavidez, A. D., DeLaRiva, A. T., Su, Y., Hofmann, J. P., Asahina, S., et al. (2019). CO oxidation by Pd supported on CeO_2(100) and CeO_2(111) facets. *Appl. Catal. B Environ.* 243, 36–46. doi:10.1016/j.apcatb.2018.10.015

Stephan, D. W., and Erker, G. (2015). Frustrated Lewis pair chemistry: Development and perspectives. *Angew. Chem. Int. Ed.* 54 (22), 6400–6441. doi:10.1002/anie.201409800

Strlckler, D. W., and Carlson, W. G. (1965). Electrical conductivity in the ZrO_2-Rich region of several M_2O_3-ZrO_2 systems. *J. Am. Ceram. Soc.* 48, 286–289. doi:10.1111/j.1151-2916.1965.tb14742.x

Sudarsan, P., and Moorthy, S. B. K. (2019). Synergistic effect of lithium and calcium for low temperature densification and grain boundary scavenging in samarium doped ceria electrolyte. *Mat. Chem. Phys.* 238, 121900. doi:10.1016/j.matchemphys.2019.121900

Sultana, S., Mansingh, S., and Parida, K. M. (2021). Crystal facet and surface defect engineered low dimensional CeO_2 (0D, 1D, 2D) based photocatalytic materials towards energy generation and pollution abatement. *Mat. Adv.* 2 (21), 6942–6983. doi:10.1039/d1ma00539a

Sun, Z., Zhang, J., Yin, L., Hu, G., Fang, R., Cheng, H.-M., et al. (2017). Conductive porous vanadium nitride/graphene composite as chemical anchor of polysulfides for lithium-sulfur batteries. *Nat. Commun.* 8 (1), 14627. doi:10.1038/ncomms14627

Suntivich, J., Gasteiger, H. A., Yabuuchi, N., Nakanishi, H., Goodenough, J. B., and Shao-Horn, Y. (2011). Design principles for oxygen-reduction activity on perovskite oxide catalysts for fuel cells and metal-air batteries. *Nat. Chem.* 3 (7), 546–550. doi:10.1038/nchem.1069

Ta, N., Zhang, M., Li, J., Li, H., Li, Y., and Shen, W. (2008). Facile synthesis of CeO_2 nanospheres. *Chin. J. Catal.* 29 (11), 1070–1072. doi:10.1016/S1872-2067(09)60002-4

Tana, Zhang, M., Li, J., Li, H., Li, Y., and Shen, W. (2009). Morphology-dependent redox and catalytic properties of CeO_2 nanostructures: Nanowires, nanorods and nanoparticles. *Catal. Today* 148 (1-2), 179–183. doi:10.1016/j.cattod.2009.02.016

Tao, X., Yang, Z., Cheng, M., Yan, R., Chen, F., Cao, S., et al. (2022). Phosphorus modulated porous CeO_2 nanocrystallines for accelerated polysulfide catalysis in advanced Li-S batteries. *J. Mat. Sci. Technol.* 131, 212–220. doi:10.1016/j.jmst.2022.06.004

Tasic, G. S., Miljanic, S. S., Marceta Kaninski, M. P., Saponjic, D. P., and Nikolic, V. M. (2009). Non-noble metal catalyst for a future Pt free PEMFC. *Electrochem. Commun.* 11 (11), 2097–2100. doi:10.1016/j.elecom.2009.09.003

Thieu, C.-A., Yang, S., Ji, H.-I., Kim, H., Yoon, K. J., Lee, J.-H., et al. (2022). Achieving performance and longevity with butane-operated low-temperature solid oxide fuel cells using low-cost Cu and CeO_2 catalysts. *J. Mat. Chem. A* 10 (5), 2460–2473. doi:10.1039/d1ta06922e

Tran, D. P. H., Pham, M.-T., Bui, X.-T., Wang, Y.-F., and You, S.-J. (2022). CeO_2 as a photocatalytic material for CO_2 conversion: A review. *Sol. Energy* 240, 443–466. doi:10.1016/j.solener.2022.04.051

Trovarelli, A., and Llorca, J. (2017). Ceria catalysts at nanoscale: How do crystal shapes shape catalysis? *ACS Catal.* 7 (7), 4716–4735. doi:10.1021/acscatal.7b01246

Urbonaite, S., Poux, T., and Novak, P. (2015). Progress towards commercially viable Li-S battery cells. *Adv. Energy Mat.* 5 (16), 1500118. doi:10.1002/aenm.201500118

Van Dao, D., Jung, H. D., Nguyen, T. T. D., Ki, S.-W., Son, H., Bae, K.-B., et al. (2021). Defect-rich N-doped CeO_2 supported by N-doped graphene as a metal-free plasmonic hydrogen evolution photocatalyst. *J. Mat. Chem. A* 9 (16), 10217–10230. doi:10.1039/d1ta01379c

Wang, H.-Y., Hung, S.-F., Chen, H.-Y., Chan, T.-S., Chen, H. M., and Liu, B. (2016). In operando identification of geometrical-site-dependent water oxidation activity of spinel Co_3O_4. *J. Am. Chem. Soc.* 138 (1), 36–39. doi:10.1021/jacs.5b10525

Wang, H., Wang, L., Luo, Q., Zhang, J., Wang, C., Ge, X., et al. (2022a). Two-dimensional manganese oxide on ceria for the catalytic partial oxidation of hydrocarbons. *Chem. Synth.* 2 (1), 2. doi:10.20517/cs.2022.02

Wang, J., Xiao, X., Liu, Y., Pan, K., Pang, H., and Wei, S. (2019a). The application of CeO_2-based materials in electrocatalysis. *J. Mat. Chem. A* 7 (30), 17675–17702. doi:10.1039/C9TA04804A

Wang, M., Shen, M., Jin, X., Tian, J., Li, M., Zhou, Y., et al. (2019b). Oxygen vacancy generation and stabilization in CeO_{2-x} by Cu introduction with improved CO_2 photocatalytic reduction activity. *ACS Catal.* 9 (5), 4573–4581. doi:10.1021/acscatal.8b03975

Wang, M., Shen, M., Jin, X., Tian, J., Shao, Y., Zhang, L., et al. (2022b). Exploring the enhancement effects of hetero-metal doping in CeO_2 on CO_2 photocatalytic reduction performance. *Chem. Eng. J.* 427, 130987. doi:10.1016/j.cej.2021.130987

Wang, M., Shen, M., Jin, X., Tian, J., Zhou, Y., Shao, Y., et al. (2020). Mild generation of surface oxygen vacancies on $CeO_{(2)}$ for improved $CO_{(2)}$ photoreduction activity. *Nanoscale* 12 (23), 12374–12382. doi:10.1039/d0nr00717j

Wang, Q., Chen, Y., Liu, X., Li, L., Du, L., and Tian, G. (2021). Sulfur doped In_2O_3-CeO_2 hollow hexagonal prisms with carbon coating for efficient photocatalytic CO_2 reduction. *Chem. Eng. J.* 421, 129968. doi:10.1016/j.cej.2021.129968

Wang, X., Ma, Y., Raza, R., Muhammed, M., and Zhu, B. (2008). Novel core-shell SDC/amorphous Na_2CO_3 nanocomposite electrolyte for low-temperature SOFCs. *Electrochem. Commun.* 10 (10), 1617–1620. doi:10.1016/j.elecom.2008.08.023

Wang, Y., Bai, X., Wang, F., Kang, S., Yin, C., and Li, X. (2019c). Nanocasting synthesis of chromium doped mesoporous CeO_2 with enhanced visible-light photocatalytic CO_2 reduction performance. *J. Hazard. Mat.* 372, 69–76. doi:10.1016/j.jhazmat.2017.10.007

Wei, T., Zhu, Y.-N., An, X., Liu, L.-M., Cao, X., Liu, H., et al. (2019). Defect modulation of Z-scheme TiO_2/Cu_2O photocatalysts for durable water splitting. *ACS Catal.* 9 (9), 8346–8354. doi:10.1021/acscatal.9b01786

Wu, T., Vegge, T., and Hansen, H. A. (2019). Improved electrocatalytic water splitting reaction on CeO_2(111) by strain engineering: A DFT+U study. *ACS Catal.* 9 (6), 4853–4861. doi:10.1021/acscatal.9b00203

Wu, Z., Li, M., Howe, J., Meyer, H. M., III, and Overbury, S. H. (2010). Probing defect sites on CeO_2 nanocrystals with well-defined surface planes by Raman spectroscopy and O_2 adsorption. *Langmuir* 26 (21), 16595–16606. doi:10.1021/la101723w

Wuilloud, E., Delley, B., Schneider, W. D., and Baer, Y. (1984). Spectroscopic evidence for localized and extended *f*-symmetry states in CeO_2. *Phys. Rev. Lett.* 53 (2), 202–205. doi:10.1103/PhysRevLett.53.202

Xia, J., Hua, W., Wang, L., Sun, Y., Geng, C., Zhang, C., et al. (2021). Boosting catalytic activity by seeding nanocatalysts onto interlayers to inhibit polysulfide

shuttling in Li-S batteries. *Adv. Funct. Mat.* 31 (26), 2101980. doi:10.1002/adfm.202101980

Xiao, D., Lu, C., Chen, C., and Yuan, S. (2018). CeO_2-webbed carbon nanotubes as a highly efficient sulfur host for lithium-sulfur batteries. *Energy Storage Mat.* 10, 216–222. doi:10.1016/j.ensm.2017.05.015

Xie, S., Wang, Z., Cheng, F., Zhang, P., Mai, W., and Tong, Y. (2017). Ceria and ceria-based nanostructured materials for photoenergy applications. *Nano Energy* 34, 313–337. doi:10.1016/j.nanoen.2017.02.029

Xing, Y., Akbar, M., Yousaf, M., Shah, M. A. K. Y., Xia, C., Gao, J., et al. (2021). CeO_2 coated $NaFeO_2$ proton-conducting electrolyte for solid oxide fuel cell. *Int. J. Hydrogen Energy* 46 (15), 9855–9860. doi:10.1016/j.ijhydene.2020.05.219

Xu, L., Huang, W.-Q., Wang, L.-L., and Huang, G.-F. (2014). Interfacial interactions of semiconductor with graphene and reduced graphene oxide: CeO_2 as a case study. *ACS Appl. Mat. Interfaces* 6 (22), 20350–20357. doi:10.1021/am5058772

Xu, Y., and Xu, R. (2015). Nickel-based cocatalysts for photocatalytic hydrogen production. *Appl. Surf. Sci.* 351, 779–793. doi:10.1016/j.apsusc.2015.05.171

Yang, C., Li, Q., Xia, Y., Lv, K., and Li, M. (2019). Enhanced visible-light photocatalytic CO_2 reduction performance of $ZnIn_2S_4$ microspheres by using CeO_2 as cocatalyst. *Appl. Surf. Sci.* 464, 388–395. doi:10.1016/j.apsusc.2018.09.099

Yang, C., Lu, Y., Zhang, L., Kong, Z., Yang, T., Tao, L., et al. (2021). Defect engineering on CeO_2-based catalysts for heterogeneous catalytic applications. *Small Struct.* 2 (12), 2100058. doi:10.1002/sstr.202100058

Yuan, Z., Peng, H.-J., Hou, T.-Z., Huang, J.-Q., Chen, C.-M., Wang, D.-W., et al. (2016). Powering lithium-sulfur battery performance by propelling polysulfide redox at sulfiphilic hosts. *Nano Lett.* 16 (1), 519–527. doi:10.1021/acs.nanolett.5b04166

Zacherle, T., Schriever, A., De Souza, R. A., and Martin, M. (2013). *Ab initio* analysis of the defect structure of ceria. *Phys. Rev. B* 87 (13), 134104. doi:10.1103/PhysRevB.87.134104

Zeng, C.-h., Xie, S., Yu, M., Yang, Y., Lu, X., and Tong, Y. (2014). Facile synthesis of large-area CeO_2/ZnO nanotube arrays for enhanced photocatalytic hydrogen evolution. *J. Power Sources* 247, 545–550. doi:10.1016/j.jpowsour.2013.09.015

Zhan, Z., and Barnett, S. A. (2005). An octane-fueled solid oxide fuel cell. *Science* 308(5723), 844–847. doi:10.1126/science.1109213

Zhang, B., Zheng, Y., Ma, T., Yang, C., Peng, Y., Zhou, Z., et al. (2021). Designing MOF nanoarchitectures for electrochemical water splitting. *Adv. Mat.* 33 (17), 2006042. doi:10.1002/adma.202006042

Zhang, J., Rao, Q., Jin, B., Lu, J., He, Q.-g., Hou, Y., et al. (2020a). Cerium oxide embedded bilayer separator enabling fast polysulfide conversion for high-performance lithium-sulfur batteries. *Chem. Eng. J.* 388, 124120. doi:10.1016/j.cej.2020.124120

Zhang, M., Chen, W., Xue, L., Jiao, Y., Lei, T., Chu, J., et al. (2020b). Adsorption-catalysis design in the lithium-sulfur battery. *Adv. Energy Mat.* 10 (2), 1903008. doi:10.1002/aenm.201903008

Zhang, S., Huang, Z.-Q., Ma, Y., Gao, W., Li, J., Cao, F., et al. (2017). Solid frustrated-Lewis-pair catalysts constructed by regulations on surface defects of porous nanorods of CeO_2. *Nat. Commun.* 8, 15266. doi:10.1038/ncomms15266

Zhang, S., Liu, Y., Zhang, M., Ma, Y., Hu, J., and Qu, Y. (2022). Sustainable production of hydrogen with high purity from methanol and water at low temperatures. *Nat. Commun.* 13 (1), 5527. doi:10.1038/s41467-022-33186-z

Zhang, S., Xia, Z., Zou, Y., Cao, F., Liu, Y., Ma, Y., et al. (2019). Interfacial frustrated Lewis pairs of CeO_2 activate CO_2 for selective tandem transformation of olefins and CO_2 into cyclic carbonates. *J. Am. Chem. Soc.* 141 (29), 11353–11357. doi:10.1021/jacs.9b03217

Zhang, W., Mohamed, A. R., and Ong, W.-J. (2020c). Z-Scheme photocatalytic systems for carbon dioxide reduction: Where are we now? *Angew. Chem. Int. Ed.* 59 (51), 22894–22915. doi:10.1002/anie.201914925

Zhang, Z., Wang, Z.-Q., Li, Z., Zheng, W.-B., Fan, L., Zhang, J., et al. (2020d). Metal-free ceria catalysis for selective hydrogenation of crotonaldehyde. *ACS Catal.* 10 (24), 14560–14566. doi:10.1021/acscatal.0c04523

Zhao, D., Pi, Y., Shao, Q., Feng, Y., Zhang, Y., and Huang, X. (2018). Enhancing oxygen evolution electrocatalysis via the intimate hydroxide–oxide interface. *ACS Nano* 12 (6), 6245–6251. doi:10.1021/acsnano.8b03141

Zhao, W., Chen, Z., Yang, X., Qian, X., Liu, C., Zhou, D., et al. (2020). Recent advances in photocatalytic hydrogen evolution with high-performance catalysts without precious metals. *Renew. Sustain. Energy Rev.* 132, 110040. doi:10.1016/j.rser.2020.110040

Zhong, S.-Y., and Gong, X.-Q. (2019). A first-principles molecular dynamics study on the surface lattice oxygen of ceria. *Appl. Surf. Sci.* 496, 143712. doi:10.1016/j.apsusc.2019.143712

Zhu, B., Liu, X., Zhou, P., Zhu, Z., Zhu, W., and Zhou, S. (2001). Cost effective yttrium doped ceria-based composite ceramic materials for intermediate temperature solid oxide fuel cell applications. *J. Mat. Sci. Lett.* 20, 591–594. doi:10.1023/A:1010900829589

Zhu, J., Tan, H., Yang, L., Dai, Z., Zhu, L., Ma, H., et al. (2020). Correction to "enantioselective synthesis of 1-aryl-substituted tetrahydroisoquinolines employing imine reductase". *ACS Catal.* 10 (1), 7–8. doi:10.1021/acscatal.9b04793

Zou, W., Shao, Y., Pu, Y., Luo, Y., Sun, J., Ma, K., et al. (2017). Enhanced visible light photocatalytic hydrogen evolution via cubic CeO_2 hybridized g-C_3N_4 composite. *Appl. Catal. B Environ.* 218, 51–59. doi:10.1016/j.apcatb.2017.03.085

Zou, Y., Zhang, M., Liu, Y., Ma, Y., Zhang, S., and Qu, Y. (2022). Highly selective transfer hydrogenation of furfural into furfuryl alcohol by interfacial frustrated Lewis pairs on CeO_2. *J. Catal.* 410, 54–62. doi:10.1016/j.jcat.2022.04.010